PRELIMINARY CONFIGURATION DESIGN OF CANNON LAUNCHED GUIDED MISSILE

by

Girish Kumar Sagoo

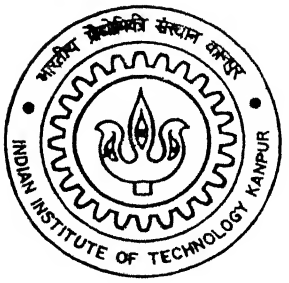

DEPARTMENT OF AEROSPACE ENGINEERING

Indian Institute of Technology Kanpur

FEBRUARY, 2003

PRELIMINARY CONFIGURATION DESIGN OF CANNON LAUNCHED GUIDED MISSILE

A Thesis Submitted
in Partial Fulfillment of the Requirements
for the Degree of

Master of Technology

by

Girish Kumar Sagoo

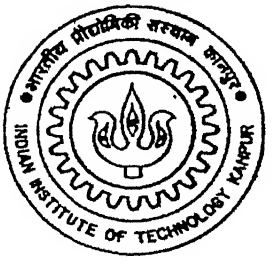

to the

Department of Aerospace Engineering
Indian Institute of Technology, Kanpur

February, 2003

CERTIFICATE

It is certified that the work contained in this thesis entitled, **"Preliminary Configuration Design of Cannon Launched Guided Missile"** by Girish Kumar Sagoo has been carried out under my supervision and that this work has not been submitted elsewhere for a degree.

(Dr. A. K. Ghosh)
Assistant Professor
Department of Aerospace Engineering
Indian Institute of Technology
Kanpur - 208016

February, 2003

ABSTRACT

A guided missile is one which is usually fired in a direction approximately to the target and subsequently receives steering command from the guidance system to improve it's accuracy .The missile being designed has both unguided as well as guided phase. During unguided phase, the missile is designed to achieve level flight at a height of 500 m up to a range of 3000 m. The guidance system becomes operational to engage the target at around 5000 m .In this work, tail deflection required to satisfy the trajectory during unguided phase has been postulated using aerodynamic coefficient generation through theoretical and wind tunnel methods. The guidance law based on proportional navigation has been used in this study. Mathematical model using non-linear aerodynamics has been proposed to calculate angle of attack and acceleration response. In order to reduce airframe response time, suitable scheme based on Stability Augmentation System (SAS) has been proposed.

ACKNOWLEDGEMENTS

With a profound sense of gratitude, I express my sincere thanks to my esteemed teachers and thesis supervisor, Dr. A. K. Ghosh for their invaluable guidance and encouragement throughout this work. I am indebted to them for exposing me into the field of Flight Mechanics and providing me with all the required facilities and help in every possible way at IIT Kanpur. I also express my sincere thanks to Dr. S. C. Raisinghani for his invaluable suggestions during this entire course of work. But for their untiring cooperation, time and patience, this work would not have seen the light of the day. Also, my due thanks to my friend Mr. Ankur Singhal for participation in data analysis.

I have no words to express my thanks to my parents, and sister, who have been a constant source of moral encouragement and inspiration to me.

I wish to thank all my friends and well-wishers who made my stay at IIT Kanpur, memorable and pleasant.

Girish Kumar Sagoo

CONTENTS

LIST OF TABLES

LIST OF FIGURES

NOMENCLATURE

A_p	= Plan form area
A_{ref}	= Reference area
AR	= Aspect ratio
a_x, a_y, a_z	= Acceleration in x, y, z direction, m/sec^2
a_c	= Normal acceleration perpendicular to the line of sight
C_L, C_d, C_m	= Non-dimensional lift, drag and pitching moment coefficients
C_l, C_n	= Rolling and yawing moment coefficient
C_N, C_A	= Coefficient of normal and axial force.
C_x, C_y, C_z	= Coefficient of axial force in x, y, z direction
C_{d0}	= Zero-lift drag coefficient
Cd_c	= Cross flow drag coefficient
d	= Diameter of the missile, mm
F_x, F_y, F_z	= Components of external forces in x, y, z directions
g	= Acceleration due to gravity, m/s^2
H_x, H_y, H_z	= Angular momentum in x, y, z direction
I_{xx}, I_{yy}, I_{zz}	= Moment of inertia about x and y & z-axis, kgm^2
k	= Gain for feedback control
$K_{f(B)}$	= Additional normal force of the fin in the presence of the body
$K_{B(f)}$	= Additional normal force on the body as result of fin being present due to angle of attack
l	= Total length of missile, m
L	= Rolling moment
m	= Mass of the missile, kg
M	= Mach number
M_N	= Cross flow mach number
M_x, M_y, M_z	= Components of external moments in x, y, z directions

N	= Yawing moment
p	= Roll rate, rad/s
P	= Ballistic Air Pressure (ambient Air Pressure), mm Hg
q	= Pitch rate, rad/s
$\overline{q}$	= Dynamic pressure, N/m^2
R_N	= Reynolds Number
r	= Yaw rate
t	= Time of flight, sec
s	= wing semi span plus body radius(r)
S	= Reference area of missile, m^2
T	= Thrust, N
u, v, w	= Velocity components in x, y and z body axes, m/s
V	= Air relative speed, m/s
W_x, W_y, W_z	= Head/tailwind, crosswind and vertical wind components, m/s
x, y, z	= Spatial coordinates, m
x_t	= x-coordinate of target
ω	= Rotation vectors
Ω	= Earth rotation angular velocity, rad/s
γ	= Flight path angle, rad
ρ	= Density of air, kg/m^3
η	= Drag proportionality factor
$\Lambda_{1/2}$	= Sweep angle, rad
λ	= Line of sight angle, rad
θ	= Pitch attitude, deg
ϕ	= Roll attitude, deg
ψ	= Yaw angle, deg
α	= Angle of attack, deg

α_f = Angle of attack seen by fin

β = Angle of sideslip, deg

δ = Tail deflection, deg

ξ = Pitch damping ratio

ω_n = Natural frequency of pitching motion

Superscripts

$\dot{}$ = Derivative with respect to time

$\rightarrow$ = Vector quantity

Subscripts

o = Initial conditions

x, y, z = Components along x, y and z direction

wind = Wind axes

sound = Sound

Stability and control derivatives

$$C_{L\alpha} = \frac{\partial C_L}{\partial \alpha}, \quad C_{Lq} = \frac{\partial C_L}{\partial (qd/2V)}, \quad C_{L\delta} = \frac{\partial C_L}{\partial \delta}$$

$$C_{m\alpha} = \frac{\partial C_m}{\partial \alpha}, \quad C_{mq} = \frac{\partial C_m}{\partial (qd/2V)}, \quad C_{N\alpha} = \frac{\partial C_N}{\partial \alpha}$$

$$C_{l\delta} = \frac{\partial C_l}{\partial \delta}, \quad C_{lp} = \frac{\partial C_l}{\partial (pd/2V)},$$

$$C_{n\beta} = \frac{\partial C_n}{\partial \beta}, \quad C_{nr} = \frac{\partial C_n}{\partial (rd/2V)},$$

$$C_{y\beta} = \frac{\partial C_y}{\partial \beta}, \quad C_{yr} = \frac{\partial C_y}{\partial (rd/2V)},$$

Chapter 1

INTRODUCTION

A missile in a simple definition may be called as a self-propelled, unmanned space or air vehicle carrying an explosive warhead. A guided missile's path can be adjusted during flight, either by automatic self-contained controls or remote human control. Guided missiles are of various types and ranges. Missiles may be aerodynamic, i.e. controlled by aerodynamic surfaces and following a straight-line trajectory to the target, or ballistic, i.e. powered during flight and following a parabolic trajectory.

Guided missiles are of various types and ranges; long-range missiles generally have nuclear warheads, while short-range missiles usually have high-explosive warheads. Aerodynamic missiles are of four types. Surface-to-Air and Air-to-Air missiles supplement anti-aircraft guns and are often guided by self-contained controls that detect and engage the target toward heat or electronic sources. Air-to-Surface missiles, launched by aircraft against ground positions, are often radio-controlled. Surface-to-Surface missiles (including ship and submarine launched versions) include many different types. All long-range missiles are ballistic; the intermediate-range ballistic missile (IRBM) can reach targets up to 1,500 nautical miles away, while the intercontinental ballistic missile (ICBM) has a range of many thousands of miles.

Guided missiles apparently had their origin in Germany. For example the Hs.298 was one of the series of German Air to Air guided missiles developed by Henschel Company during world war II [1]. The Hs.298, which was radio controlled from parent aircraft, was to be released either slightly above or below the target. Apparently the

height differential made it easier to aim and guide the missile. On December 22, 1944 three missiles were test flown from JU 88 G aircraft. All three tests were a failure. The Rheintocter (R-1) was a Surface to Air missile, developed in Germany during World War II. This unusual looking two stage radio controlled missile weighed nearly 4000 lb and had three sets of plywood fins: one for the booster and two for the sustainer. The missile was ineffective because allied bombers, which were the R-1's intended target, flew above the range (20,000 ft) of this surface to air missile.

Although the Germans apparently knew the proportional navigation during the World War II, no applications on the Hs .298 or R-1 missiles using proportional navigation were reported [2] .The Lark missile, which had its first successful flight test in December 1950, was the first missile to use proportional navigation. Since that time proportional navigation guidance has been used in virtually all the world's tactical radar, Infra Red (IR) and television (TV) guided missiles[3]. The popularity of this interceptor guidance law is based on its simplicity, effectiveness and ease of implementation. Apparently C.Yuan and others first studied proportional navigation at RCA laboratories during World War II under the auspices of U.S Navy [4].

Guidance is the process of guiding the path of an object towards a given point, which may generally be moving. If the given point, which we call as target, is fixed, e.g., a seaport then the process is usually called navigation. If the target moves in a way that is not predictable –for example, an aircraft evading ground to air missiles-then the process is Guidance in it's narrower sense.

The guidance law was conceived from physical reasoning and equipment available at that time. Proportional navigation was extensively studied at Huges Aircraft

Company [5] and implemented in a tactical missile using pulse radar system. Finally a proportional navigation was fully developed at Raytheon and implemented in a tactical continuous wave radar homing missile [6].

After World War II, the U.S work on proportional navigation was declassified and first appeared in the journal of applied physics[7]. Mathematical derivation of the 'optimality' of the proportional navigation came more than twenty years later[8] .

Theoretically the proportional navigation guidance law issues acceleration commands, perpendicular to instantaneous missile-target line of sight, which are proportional to the line of sight rate and closing velocity. In tactical radar homing missiles using proportional navigation guidance, the seeker provides the line of sight rate information. In tactical missile proportional navigation guidance are usually implemented by moving the fins or other control surfaces to obtain the required acceleration.

Conventionally, the artillery tank gun uses unguided projectile to neutralize enemy tank. The operational range for such tank is well with in 3 km. The projectile or shell fired from the tank gun is subjected to higher level of acceleration, non-standard atmospheric conditions and thus many times the accuracy in terms of 'first shot kill' deteriorates.

From last ten years, considerable efforts are being directed to develop guided anti-tank ammunition. Due to strategic reasons no open literature is made available for ready reference.

Armament Research & Development Establishment (ARDE), Pune has undertaken a task of developing anti-tank guided missile. The subject missile is being developed to meet the following requirements:

1.Given maximum elevation of around 10 deg, the missile should be able to reach a height of around 500 m within a minimum possible time.

2.At around 500 m, the missile should maintain almost level flight up to 3 km of range.

3.At around 3 km range, once the guidance system is made active, the missile should be capable of engaging a target at a maximum distance of 2 km using appropriate guidance control law technique.

The first requirement demands large turning rate of the missile. Since during this phase booster will be on, part of this turning rate will be obtained from thrust and part from lift force generated by the missile at a particular angle of attack. To utilize part of the thrust and lift force, it is necessary to introduce angle of attack to the missile. The control fins at the rear end of the missile can be appropriately deflected to generate the required angle of attack. Since during this phase no guidance and control are operative, tail deflection has to be pre-programmed as a function of time to generate required angle of attack.

The second requirement to maintain level flight at around 500 m demands that the missile must maintain a predefined angle of attack to balance the weight up to a range of 3 km. Here again the tail control deflection has to be pre-programmed to generate adequate angle of attack to produce desired lift.

To meet the third requirement, the missiles are configured in such a manner, that it generates sufficient acceleration per unit tail deflection to steer the missile towards the target.

The strategic missile with terminal guidance needs to have a high level of maneuverability capability at terminal end. In aerodynamic sense it means that the

missile should have marginal static stability at the operational angle of attack. The missile in question does not have an attached wing as lifting surface and during terminal phase thrust is not available, thus most of the lift is to be generated by the blunt shaped cylindrical body. The cylindrical body at high angle of attack, generate complex vortex pattern to add non-linearity to the flow[9]. The fin attached to the rear end of the missile frequently falls in the 'vortex sheet' created by the body. Interaction of these vortices with the flow near the fin alters the lifting characteristics significantly. More importantly physical phenomenon governing this interaction is not well understood or modeled[9]. Further at high angle of attack, the body is expected to shed asymmetric vortices, which drastically alters the flow field around the fin. Available theoretical methods find it difficult to predict this behavior and thus wind tunnel testing remains the best source to capture the flow non- linearities and its effect in forces and moments experienced by the missile[10]

Accurate values of the forces and moments are a paramount importance to pre-program the tail deflection to achieve the desired trajectory and evolve efficient control law to implement guidance command. Of course need for an approximate theoretical estimation of these forces and moments is absolutely necessary to freeze initial parameters of the missile. To refine the design parameters, wind tunnel testing is routinely done. Thus as a part of this thesis, aerodynamic parameters were estimated using the both wind tunnel testing and theoretical methods.

The full scale model fabricated by ARDE, Pune was tested in National Wind Tunnel Facility at IIT Kanpur.To ensure, sufficient rigidity to the sting, supports mounts were fabricated as a part of this exercise. The wind tunnel test data was generated for

different combinations of angle of attack and tail deflection. Finally comparisons were made between theoretical and wind tunnel estimates. It was generally observed that theoretical and wind tunnel estimates compares fairly well as long as angle of attack was kept between –15 deg to +15 deg. The wind tunnel data clearly brought out the effect of shedding vortices at high angle of attack, which as expected theoretical methods failed to capture.

Once the aerodynamic parameters were frozen based on this study, next step was to formulate the trajectory model. Trajectory model was formulated using six degree of freedom model to predict range and height of the missile for a given elevator deflection and initial conditions. Different tail (elevator) deflections were given as input to the trajectory model to obtain the desired trajectory.

As discussed earlier, to implement proportional navigation, kinematics of the problem demands specified amount of accelerations to be made available. Thus, at the design stage, the normal acceleration produced per unit tail deflection is obtained using short period approximation[11]. Non-linear model[10] was assumed to calculate steady state angle of attack and normal acceleration. Next, the normal acceleration obtained was compared with acceleration required as per proportional navigation kinematics to freeze the amount of tail deflection required for terminal guidance. The normal acceleration is computed assuming the steady state value of α i.e. (α_{trim}) for particular tail deflection δ. However since these missiles are designed to have low static stability (for high maneuverability), the pitch damping is very low and thus takes longer time to reach steady state value of α_{trim} to generate required normal acceleration. This is highly undesirable from implementation point of view. Thus a need is arised to artificially damp

the missile dynamics without altering the steady state trim value. Hence, as the final work of this progress, preliminary stability augmentation scheme has been proposed for implementation.

Chapter 2 discusses in detail the theoretical methods employed and the conduct of wind tunnel testing. Chapter 3 discusses strategy development to pre-program tail deflection to satisfy the first missile requirement. Chapter 4 presents scheme to engage target using proportional navigation. Further, theory employed to generate accelerations through tail deflections has been discussed in detail. It also discusses the method to design artificial stability augmentation system (SAS) to artificially damp the missile dynamics. Finally, in chapter 5 the conclusion and scope for future work have been discussed.

Chapter 2

ESTIMATION OF AERODYNAMIC PARAMETERS

2.1 GENERAL

The conventional approach hitherto for understanding the flight behavior of missiles is to develop mathematical models that could predict all elements of the trajectory from launch to target. To this purpose it becomes essential that all the forces, moments affecting the flight of the missile be accounted in a well-defined mathematical form[11]. Beginning with the most simple but relatively inaccurate model, the in-vacuo trajectory model, more and more sophisticated models of increasing accuracy such as point mass model (PMM), the modified point mass model (MPMM) and six degrees of freedom model (SDFM) have been developed. These models require aerodynamic coefficients as input.

There are three distinct approaches for estimating aerodynamic parameters:

1. Theoretical methods
2. Wind Tunnel Testing
3. Flight Testing

At the primary design stage of any system, theoretical methods[10, 12,13] are useful in spite of their limited accuracy. The wind tunnel testing improves the accuracy of estimation but it is time consuming and expensive way of estimating the aerodynamic parameters. Precise simulation of control surfaces, power effects, and flight condition is difficult. The model tested in the wind tunnel is generally slightly different from actual

flight due to last minute configuration changes. Other reasons of discrepancies between flight and wind tunnel results are Reynolds number discrepancies and interference due to support system. It is therefore, desirable that the wind tunnel estimates be corroborated with the estimates from actual flight test data.

In the present work, the aerodynamic coefficients were obtained using theoretical methods and wind tunnel testing. The model being tested is having a blunt nose with cylindrical after body. The fins attached to the rear part of the body is having tapered configuration. There are also noticeable gaps between the fin base and cylindrical surface. The missile being a tail controlled (no wing) needs large angle of attack to generate sufficient normal lift for maneuver. Hence, in general the forces and moment generated on the missile will be highly non-linear in nature. Further, at high angle-of-attack, the body will shed vortices and subsequently these vortices will interact non-linearly with flow field around the tail [9]. The theoretical method needs to be powerful enough to capture both linear and nonlinear behavior. Any theoretical methods will find it difficult to estimate aerodynamic parameters accurately for such model configuration. Thus, extensive wind tunnel testing is necessary to arrive at the final configuration. Details of the theoretical methods and wind tunnel testing that were used to estimate force coefficient are given in the subsequent paragraph.

2.2 DESCRIPTION OF THEORETICAL METHODS TO ESTIMATE FORCE AND MOMENT COEFFICIENT

2.2.1 BODY ALONE

There are many non-linearities that occur in the weapon aerodynamics. The ones that have most influence on the body alone are angle of attack, mach number, crossflow reynolds number and asymmetric vortices. This entire phenomenon can be properly modeled in an approximate sense except asymmetric shedding vortices.

Normal force coefficient can be written as

$$(C_N)_{Body} = (C_N)_{Body,lin} + (C_N)_{Body,nonlin} \tag{2.1}$$

$(C_N)_{Body,lin}$ can be approximated using munk factor[12] $(k_2 - k_1)$. However this approach is strictly valid for slender body with lifting nose.

The missile under investigation has slenderness ratio of around 8.33 with blunt nose. The theoretical estimates are going to be inferior for such a "blunt nose slender body". Due to non-availability of any other methods, $(C_N)_{body,lin}$ has been computed using munk factor obtained through Fig. 2.2.1 below.

$$(C_N)_{Body,lin} = 2.(k_2 - k_1) \tag{2.2}$$

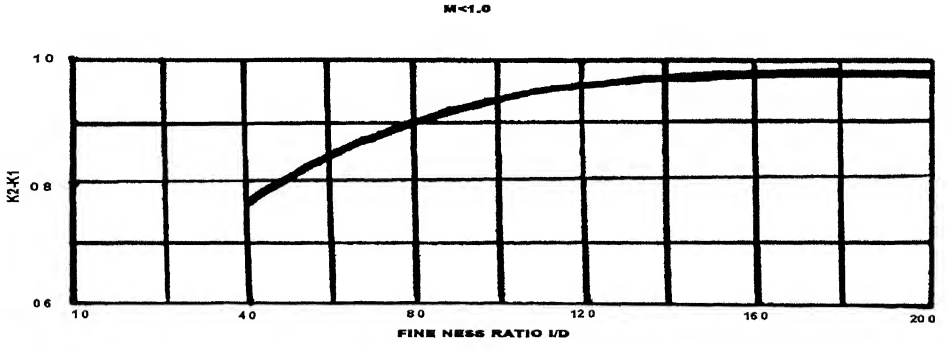

Fig. 2.2.1 Variation of Munk Factor with fineness ratio

$(C_N)_{Body,nonlin}$ is a cross flow term based on drag force experienced by an element of circular cylinder of same diameter in a stream moving at the cross component of the stream velocity $V_\infty \sin\alpha$ .The cross flow term is primarily created by the viscous effects of the fluid as it flows around the body, often separating and creating a nonlinear force coefficient. The non-linear coefficient (C_N) can be approximated by

$$(C_N)_{Body,nonlin} = \eta Cd_c . \frac{A_p}{A_{ref}} . \sin^2 \alpha \tag{2.3}$$

where

$$\eta = \frac{(1-\eta_0)}{1.8} . M_N + \eta_0 \tag{2.4}$$

A_p =Plan form area; A_{ref} =Reference area

$$M_N = M \sin\alpha \tag{2.5}$$

η used in the above expression is the drag proportionality factor or the ratio of crossflow drag of a cylinder of finite length to one of infinite length. This variation[10] is graphically presented in Fig. 2.2.2.

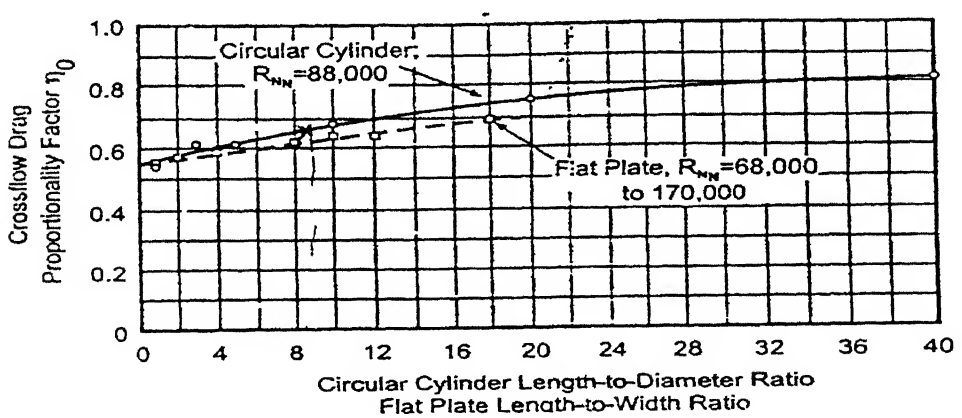

Fig. 2.2.2 Ratio of cross flow drag coefficient for a finite length cylinder (or flat plate) to that for infinite length cylinder (or flat plate) at $M_N = 0$

Procedure for Cd_c calculation:

The cross flow drag coefficient Cd_c can be computed as a function of M_N using Fig 2.2.3.

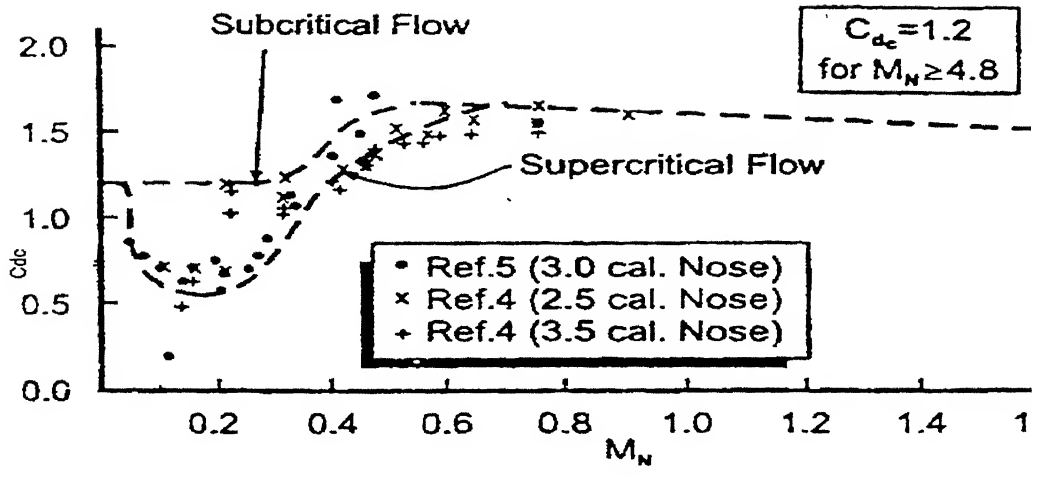

Fig. 2.2.3 Variation of cross flow drag coefficient with cross flow Mach number

It is important to identify the nature of flow i.e. sub critical or super critical for estimation of cross flow drag coefficient Cd_c. Using the following conditions could be used to identify the nature of the flow.

Super critical:

If $R_{N_{effective}} > R_{NC}$

$M_N > M_{NC}$

Sub critical:

If $R_{N_{effective}} < R_{NC}$

$M_N < M_{NC}$

where R_{NC} = 180,000 and M_{NC} = 0.1 have been assumed[10].

Thus knowing the values of η and Cd_c for a given mach number and angle of attack, C_N could easily be calculated using eq. (2.1).

To locate the point of application of this force, the center of pressure at subsonic speed has been assumed to be at the centroid of the planform area[10]. The center of pressure moves aft /forward with angle of attack/mach number. The variation of center of pressure for body alone can be computed using the data base given in Ref.(10). The database used for this case is presented in tabular form in table 2.2.1 for ready reference.

Table 2.2.1 Shift in body alone center of pressure as a function of Mach number and angle-of-attack (as a fraction of body length)

Shift in body-alone center of pressure as a function of Mach number and AOA (as a fraction of body length)										
M\a	0	10	20	30	40	50	60	70	80	90
0 00	0.00	0 01	0.01	0.000	−0.025	−0.040	−0.040	−0.030	−0.010	0.00
0.20	0 00	0.02	0.02	0.010	−0.025	−0.040	−0.045	−0.030	−0.010	0 00
0.40	0.00	0.03	0.03	0.010	−0.025	−0.040	−0.050	−0.030	−0.015	0.00
0 60	0 00	0.03	0.03	0.010	−0.035	−0.055	−0.070	−0 050	−0.030	0.00
0.80	0.00	0.02	0.02	−0.015	−0.050	−0.070	−0.070	−0.050	−0.015	0.00
0.90	0.00	0.00	0 00	−0.015	−0.050	−0.070	−0.070	−0.040	−0.015	0.00
1.00	0.00	0.00	0.00	−0.015	−0.040	−0.040	−0.040	−0.030	−0.005	0.00
1.15	0 00	0 00	0.00	−0.015	−0.020	−0.025	−0 030	−0.025	−0.005	0 00
1.30	0.00	0 00	0 00	−0 005	−0.010	−0 010	−0.010	−0.005	0.000	0.00
1 50	0.00	0.00	0 00	0.000	0.000	0.000	−0 005	−0 005	0 000	0 00
2 00	0.00	0.02	0 02	0.020	0.015	0 010	0 005	0.000	0.000	0 00
2.50	0 00	0.03	0.03	0.030	0.015	0.010	0 005	0.000	0 000	0.00
6.00	0.00	0.03	0.03	0.030	0.015	0.010	0 005	0.000	0.000	0 00
20 00	0 00	0.00	0.00	0.00	0.00	0.00	0.00	0.000	0.000	0 00

2.2.2 FIN ALONE NORMAL FORCE COEFFICIENT

The fourth order equation for the fin alone normal force was found to be most accurate for all angle-of-attack[10] .The fin alone normal force coefficient is thus defined as

$$(C_N)_{fin} = a_0 + a_1\alpha_f + a_2{\alpha^2}_f + a_3{\alpha^3}_f + a_4{\alpha^4}_f \tag{2.6}$$

where

$\alpha_f = |\alpha + \delta|$ and δ is the fin setting angle.

To predict the fin alone normal force coefficient, the equation requires these five constants to be evaluated. Thus five independent equations or conditions are needed. The first condition to evaluate a_0 is that most weapon lifting surfaces are symmetric and have zero camber. As a result normal force at zero angle of attack is zero.

Thus

$$a_0 = 0 \tag{2.7}$$

and

$$a_1 = (C_{N\alpha})_{\alpha=0} \tag{2.8}$$

which is evaluated using[10]

$$a_1 = (C_{N\alpha})_{\alpha=0} = \frac{2\Pi.AR}{2 + \left[AR^2(\beta^2 + \tan^2 \Lambda_{1/2}) + 4\right]^{\frac{1}{2}}} \tag{2.9}$$

where

$$\beta = \sqrt{1 - M^2}$$

The other coefficients a_2, a_3 and a_4 can be evaluated using the following expressions[10]

$$a_2 = 34.044(C_N)_{\alpha=15^0} - 4.824(C_N)_{\alpha=35^0} + 0.426(C_N)_{\alpha=60^0} - 6.412a_1 \tag{2.10}$$

$$a_3 = 88.240(C_N)_{\alpha=15^0} + 23.032(C_N)_{\alpha=35^0} - 2.322(C_N)_{\alpha=60^0} + 11.464a_1 \tag{2.11}$$

$$a_4 = 53.219(C_N)_{\alpha=15^0} - 17.595(C_N)_{\alpha=35^0} + 2.661(C_N)_{\alpha=60^0} - 5.971a_1 \tag{2.12}$$

The terms $(C_N)_{\alpha=15^0}, (C_N)_{\alpha=35^0}, (C_N)_{\alpha=60^0}$ are the normal force coefficients at $\alpha_f = 15^0, 35^0, 60^0$ respectively as a function of Mach number, taper ratio and aspect ratio. The numerical value of these coefficients as function of Mach number, taper ratio and aspect ratio are tabulated in Appendix A, Table 2(A).

2.2.3 FIN BODY AND BODY FIN INTERFERENCE

There are many types of interference effects that can occur in aerodynamics. First of all, when a fin body configuration is present, there is an additional pressure load induced on the body as a result of fin being present and likewise, there is an additional pressure load induced on the fins as a result of being in the presence of body. Another type of interference is that due to the body shed vortices as they affect the fin surface.

There are two primary types of interference $K_{f(B)}$ and $K_{B(f)}$. These are interference factors associated with normal force of the fin in the presence of the body and additional normal force on the body as result of fin being present due to angle of attack.

Mathematically

$$K_{f(B)} = \frac{C_{N_{f(B)}}}{(C_N)_{fin}} \tag{2.13}$$

and defined as Ratio of normal force coefficient of fin in presence of body to that of fin alone at $\delta = 0$ deg.

$$K_{B(f)} = \frac{\Delta C_{N_{B(f)}}}{(C_N)_{fin}} \tag{2.14}$$

and is defined as ratio of additional body normal force coefficient in the presence of fin to fin alone normal force coefficient at $\delta = 0$ deg.The mathematical model to estimate $K_{f(B)}$ and $K_{B(f)}$ are presented next for ready reference [10].

MATHEMATICAL MODEL FOR $K_{f(B)}$

$$K_{f(B)} = \left[K_{f(B)}\right]_{SBT} + \left[\Delta K_{f(B)}\right]_{\alpha=0} \quad ; \qquad \alpha \le \alpha_C \tag{2.15}$$

$$K_{f(B)} = \left[K_{f(B)}\right]_{SBT} + \left[\Delta K_{f(B)}\right]_{\alpha=0} + \left|(|\alpha| - \alpha_C)\right| . \frac{dK_{f(B)}}{d\alpha} \quad ; \qquad \alpha_C < \alpha \le \alpha_D \tag{2.16}$$

$$K_{f(B)} = 1 - \left(\frac{\alpha_M - |\alpha|}{\alpha_M - \alpha_D}\right)\left(1 - \left[K_{f(B)}\right]_{\alpha=\alpha_D}\right) \quad ; \qquad \alpha_D < \alpha \le \alpha_M \tag{2.17}$$

$$K_{f(B)} = \left[K_{f(B)}\right]_{\alpha=\alpha_M} ; \qquad \alpha > \alpha_M \tag{2.18}$$

$$\frac{dK_{f(B)}}{d\alpha} = \frac{\left[K_{f(B)}\right]_{\alpha_D} - \left[K_{f(B)}\right]_{\max}}{\alpha_D - \alpha_C} \tag{2.19}$$

$$\left[K_{f(B)}\right]_{\max} = \left[K_{f(B)}\right]_{SBT} + \left[\Delta K_{f(B)}\right]_{\alpha=0} \tag{2.20}$$

MATHEMATICAL MODEL FOR $K_{B(f)}$

$$K_{B(f)} = \left[K_{B(f)}\right]_{SBT} + \left[\Delta K_{B(f)}\right]_{\alpha=0} + |\alpha| . \frac{dK_{f(B)}}{d\alpha} ; \qquad \alpha \le \alpha_1 \tag{2.21}$$

$$K_{B(f)} = \left[K_{B(f)}\right]_{\alpha=\alpha_1} + \left(\frac{\alpha_1 - |\alpha|}{\alpha_2 - \alpha_1}\right)\left\{\left[K_{B(f)}\right]_{\alpha=\alpha_1} - \left[K_{B(f)}\right]_{\min}\right\} \quad ; \ \alpha_1 < \alpha \le \alpha_2 \tag{2.22}$$

$$K_{B(f)} = \left[K_{B(f)}\right]_{\min} ; \ \alpha \ge \alpha_2 \tag{2.23}$$

$$\left[K_{f(B)}\right]_{SBT}=\frac{2}{\pi}\left\{\frac{\left(1+\frac{r^4}{s^4}\right)\left[\frac{1}{2}\tan^{-1}\frac{1}{2}\left(\frac{s}{r}-\frac{r}{s}\right)+\frac{\pi}{4}\right]}{\left(1-\frac{r}{s}\right)^2}-\frac{\frac{r^2}{s^2}\left[\left(\frac{s}{r}-\frac{r}{s}\right)+2\tan^{-1}\frac{r}{s}\right]}{\left(1-\frac{r}{s}\right)^2}\right\} \tag{2.24}$$

$$\left[K_{B(f)}\right]_{SBT}=\left(1+\frac{r}{s}\right)^2-\left[K_{f(B)}\right]_{SBT} \tag{2.25}$$

The data base to estimate $\left[\Delta K_{f(B)}\right]_{\alpha=0}$, α_C, $\left[K_{f(B)}\right]_{\alpha=\alpha_D}$, α_D, α_M, $\left[\Delta K_{B(f)}\right]_{\alpha=0}$, $\frac{dK_{f(B)}}{d\alpha}$, α_1, α_2 for different combination of is a function of aspect ratio, taper ratio and Mach number are enclosed in Appendix 'A', Table 2(B).

Thus the normal force coefficient for the complete body and fin incorporating interference factors can be written as:

$$C_N=(C_N)_{Body}+(C_N)_{fin}.(K_{f(B)}+K_{B(f)}).\frac{A_{fin}}{A_{ref}} \tag{2.26}$$

CENTER OF PRESSURE OF MISSILE

Total center of pressure of the missile is estimated using the following relation

$$(Xcp)_{missile}=\frac{C_{N,lin}.X_1+C_{N,nonlin}.X_2+C_{N,fin}.X_3}{C_{N,lin}+C_{N,nonlin}+C_{N,fin}} \tag{2.27}$$

where

X_1=Center of pressure for nose linear loads ≈ 0.6 nose lengths.

X_2=Center of pressure of non-linear body load .The non-linear center of pressure shifts with angle of attack.

X_3 =Center of pressure for fin, is assumed to be at the quarter chord point(c/4). Its variation with angle of attack has been neglected.

Total moment coefficient has been obtained by taking moment about the missile center of gravity.

$$(C_m)_{cg} = -\frac{[C_{N_{lin}}.(X_1 - X_{cg}) + C_{N_{nonlin}}.(X_2 - X_{cg}) + C_{N_{fin}}.(X_3 - X_{cg})]}{d} \quad (2.28)$$

2.3 DESCRIPTION OF WIND TUNNEL TESTING TO ESTIMATE FORCE AND MOMENT COEFFICIENTS

In any wind tunnel testing, the accuracy of wind tunnel estimates strongly depends on the exactness of the model, precise mounting to simulate test conditions and of course accurate calibration of data acquisition system.

Armament Research & Development Establishment (ARDE), Pune , supplied the full-scale model for design evaluation, analysis and exhaustive wind tunnel testing. The schematic of the model used for testing is presented in Fig. 2.3.1. The major dimensions of the model are not mentioned for the sake of secrecy.

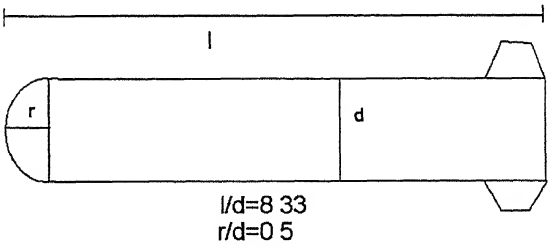

Fig 2.3.1 Schematic of the model used for design evaluation and testing.

The objective behind the wind tunnel testing of this model was to estimate force and moment coefficient at speed of around 60m/s for various combination of angle-of-attack (α) and tail setting angle (δ). For a fixed tail settings, the angle-of-attack was varied from -15° to 45°. Tests were repeated for various angles of tail setting angles ranging from $+10^{\circ}$ to -40°. '+' is the tail down and ' - ' is the tail up movement.

The full-scale model was tested at National Wind Tunnel Facility (NWTF), at IIT Kanpur. The sting available in this tunnel was not sufficient to give required large angle-of-attack by rotating the model in vertical plane. Hence, a new methodology was adopted for testing the model. Angle-of-attack was simulated using two vertically located turntables in the test section. The model was placed between these turn tables. A fitment as described in Fig. 2.3.2 was fabricated to hold the model rigidly between these turn tables. To avoid interference due to wake formation by the fitment, the model was positioned at a sufficiently large distance from the vertical element of the fitment.

A six-component balance was installed inside the model to measure forces and moments. The tunnel was stabilized at a wind speed of 60 m/sec and data acquisition system was switched on to acquire data for three missile configuration namely, body-alone, body with fins at zero settings in '+' configuration, and body with fin at different positive (down) and up (negative) fin setting angles. Before every run, a dry run (no wind) was conducted to estimate the bias error, if any. The raw data acquired were then processed to obtain desired force and moment coefficients namely $C_X, C_Y, C_N, C_m, C_n, C_l$. The detail procedure followed for processing wind tunnel raw data is given in Appendix"B".

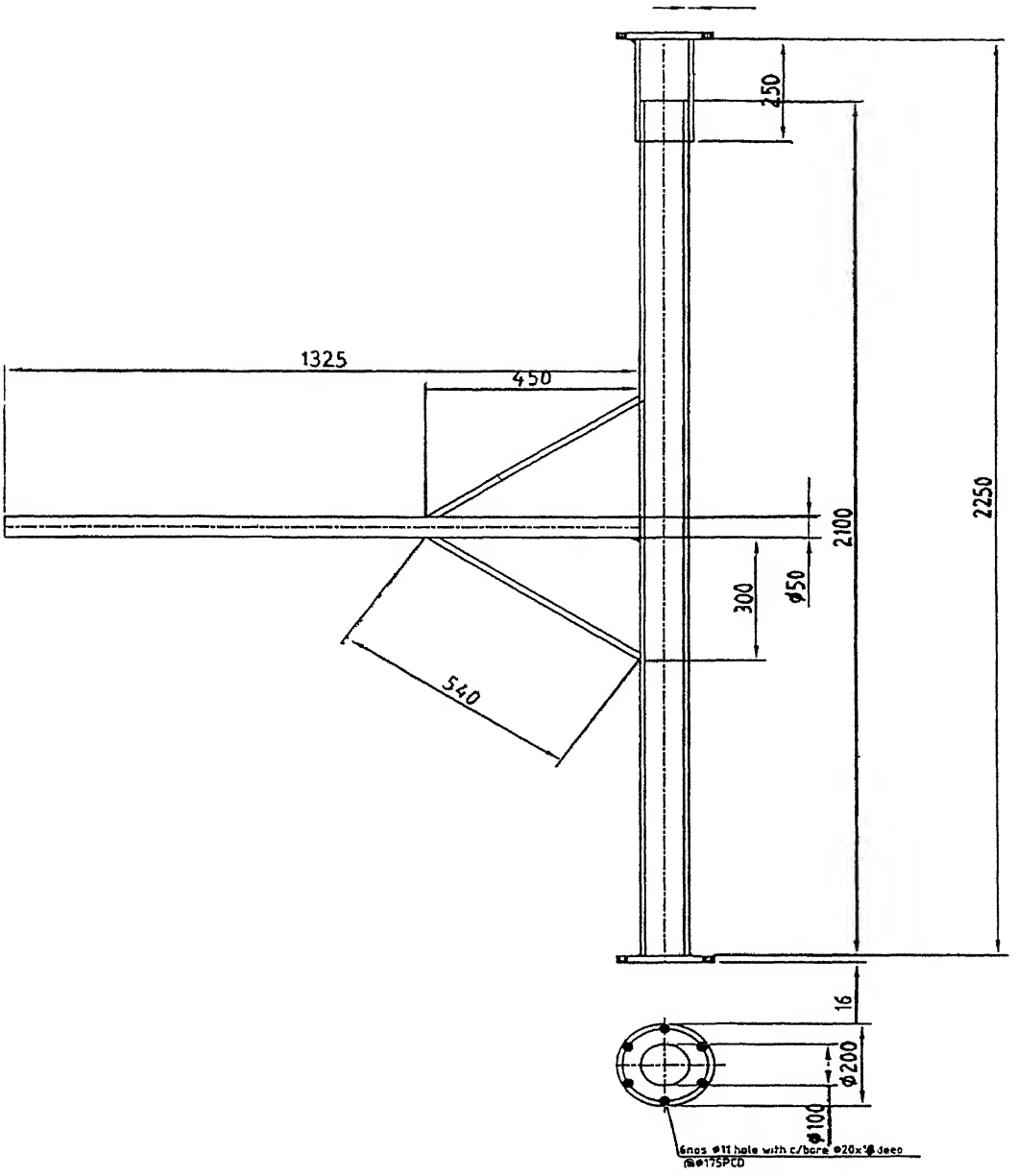

Fig 2.3.2 Schematic of fitment fabricated to hold the model.

2.4 RESULTS AND DISCUSSION ON ESTIMATION OF AERODYNAMIC PARAMETERS USING THEORETICAL AND WIND TUNNEL METHODS

2.4.1 WIND TUNNEL TESTING

The force and moments coefficients were obtained using wind tunnel data. The wind tunnel raw data was processed, corrected for bias and then corrected to non-dimensional form to get aerodynamic coefficients $C_X, C_Y, C_N, C_m, C_n, C_l$.

Wind tunnel data for three-missile configurations-body alone, body with fins at zero settings in '+' configuration, and body with fin at different positive (down) and negative (up) fin settings are analyzed in this section. All these configurations were used to record data with α varying from –15° to 45°.

The Normal force (C_N) and Pitching moment (C_m) variation with angle-of-attack for varying fin angle settings (δ).

The Normal Force: For body alone, Fig. 2.4.1 shows that C_N Vs α variation is nearly linear in the range of α from –15° to 45°. A positive value of C_N is observed at α = 0 while the corresponding C_m is negative (-0.0115). Because the center of pressure of body is ahead of c.g, a positive value of C_N and negative C_m are inherently inconsistent. To check our conjecture that this inconsistency is due to error in zero setting of α, a plot of C_N for α -5° to 5° was plotted and joined by a straight line. The intersection of this straight line with C_N axis at α = 0 showed C_N = –0.018. Thus, the C_N and C_m values are consistent in sign: A negative C_N ahead of c.g producing a negative C_m.

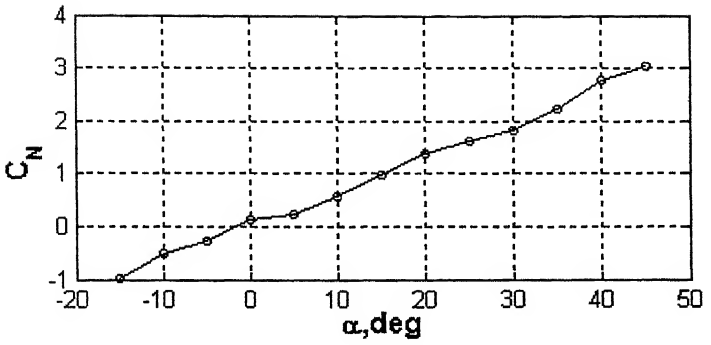

Fig. 2.4.1 Normal force coefficient for body alone configuration

It may be mentioned that the $\alpha = 0$ setting for body plus fin combination was redone afresh, it seems that the new setting of α yielded C_N (-0.098) and C_m (0.0147) values, which are consistent. This further suggests that the inconsistency of C_N and C_m for body alone was probably due to $\alpha = 0$ setting only.

C_N Vs α at $\delta = 0$: Figure 2.4.2 shows that the C_N Vs α is almost linear till α=10°, and then non-linear contribution is almost as much as the linear contribution till α=20°. At α=20°, there seems to be break in the trend and a new non-linear behavior is observed. At α=10°, $\delta = 0$ C_N was measured to be 0.829. Also, the measured value of C_N for body alone at α=10° was 0.555. These numerical values will be compared next with the measured values at different α and δ combinations.

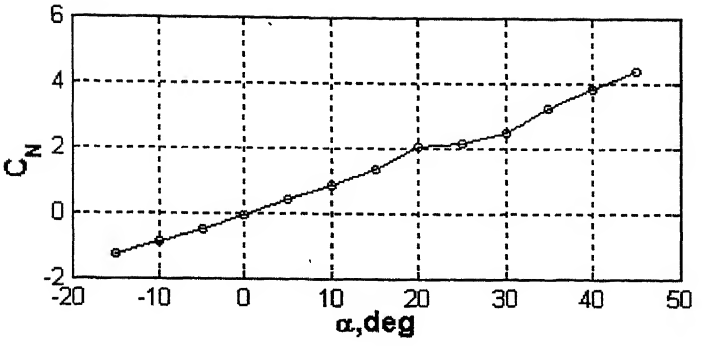

Fig. 2.4.2 Normal force coefficient for body and fin at cant = 0 deg.

C_N Vs α at $\delta \neq 0$: Figure 2.4.3 shows the trend for $\delta = -10^\circ$. It has a trend of C_N variation with α similar to the one observed for $\delta = 0$.

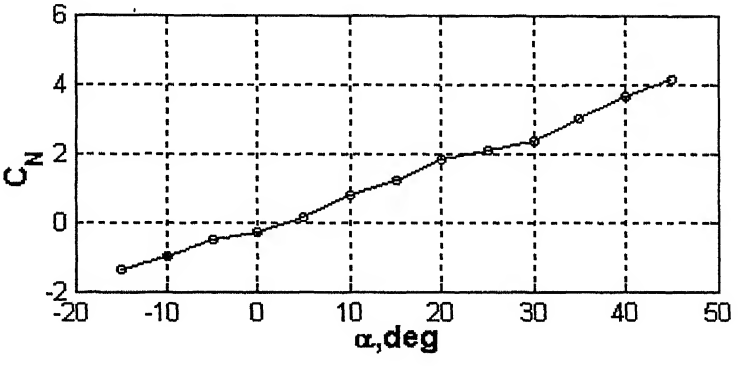

Fig. 2.4.3 Normal force coefficient for body and fin at cant = -10 deg.

The measured C_N at α=10° and δ= -10° was 0.797. One would expect that at this combination of α and δ ,fin contribution to C_N is zero and C_N would have value equal to that for body alone at α=10° i.e. C_N =0.555 .However , the measured value is actually comparable to 0.829 measured for body plus fin at α=10° .It is known that for long slender bodies, flow separation and shedding of trailing vortices begins from the body at some distance from the nose of the body and this vortex flow would interact with fins to generate normal force .This we believe explains the observed value of C_N The variations of measured C_N with α for δ= -20° ,-25° ,-30° are presented in

Fig.2.4.4-2.4.6. Again, as in case of α=10° and δ= -10, the combination of (α=20° and δ= -20°), (α =25° and δ= -25°) and (α =30° and δ= -30°) show that measured values of C_N values greater than that for body alone at the corresponding α. Here again, it seems to confirm our earlier conjecture that vortex flow is responsible for additional C_N .In an overall way, the variation of C_N with α for all these δ settings are similar in character as discussed for δ =0 case.

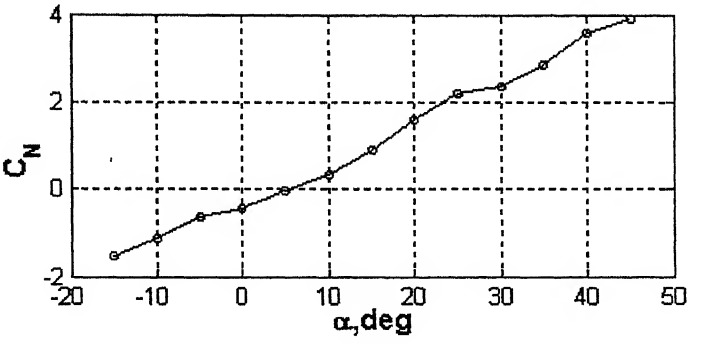

Fig. 2.4.4 Normal force coefficient for body and fin at cant = -20 deg.

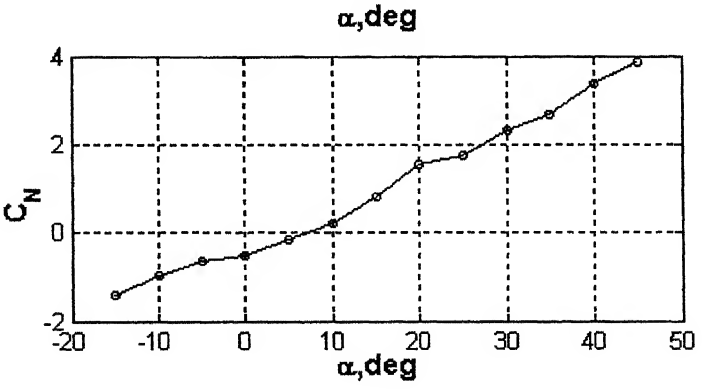

Fig. 2.4.5 Normal force coefficient for body and fin at cant = -25 deg.

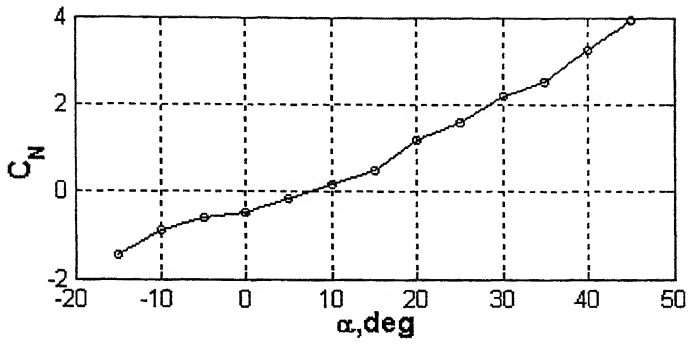

Fig. 2.4.6 Normal force coefficient for body and fin at cant = -30 deg.

The Pitching moment:

For body alone, Fig 2.4.7 shows that the variation of C_m Vs α is increasing almost linearly up to $\alpha = 10^\circ$, and then non-linearly till $\alpha = 30^\circ$, beyond which the C_m decreases.

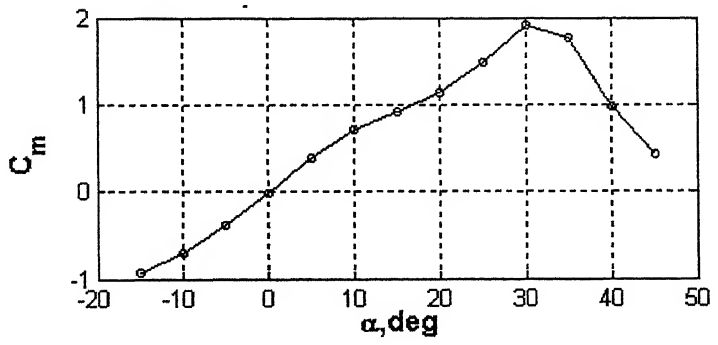

Fig. 2.4.7 Pitching Moment coefficient for body alone configuration.

It was noted earlier that the normal force (body) increases with α even beyond α=30°.This would suggest that the decrease in C_m is due to a shift of the center of pressure closer to C.G.

C_m Vs α for $\delta = 0$: Figure 2.4.8 shows that the missile is stable till α=10° but as α varies

between 10° to 30°, the missile attains almost neural stability and then again beyond α=30°, it becomes stable (more stable than at α<10°).

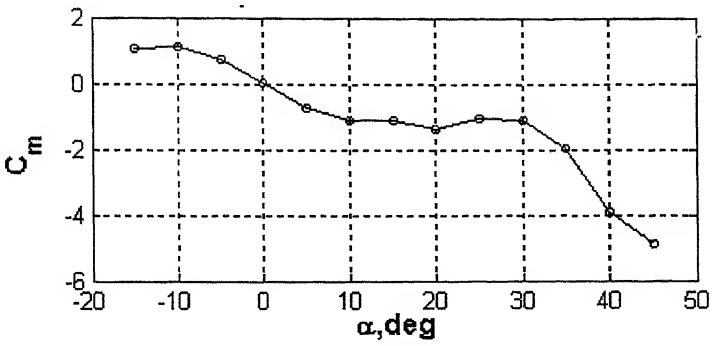

Fig. 2.4.8 Pitching Moment coefficient for body and fin at cant = 0 deg.

It was pointed out that body alone contribution increases till α =30° and then drops off. The reason for achieving neutral stability in the range of $10° < \alpha < 30°$ seems to be a result of well designed tail size and its location. For efficient maneuvering, it is desirable that the missile has a low or almost neutral stability in the range of α that is likely to be used during maneuvers. The C_m contribution from the fin and body are made to cancel each other; the C_m (negative contribution) due to fin increases as α increases but so also the body contribution (positive) increases with α. Now by clever design of fin, it is ensured that both contributions cancel each other. This is achieved for values of α up to 30°. However, as mentioned earlier for $\alpha > 30°$, the unstable contribution to C_m due to body drops off and thereby the net C_m again is increasingly negative as α increases, and missile becomes stable again.

C_m Vs α for $\delta < 0°$:.

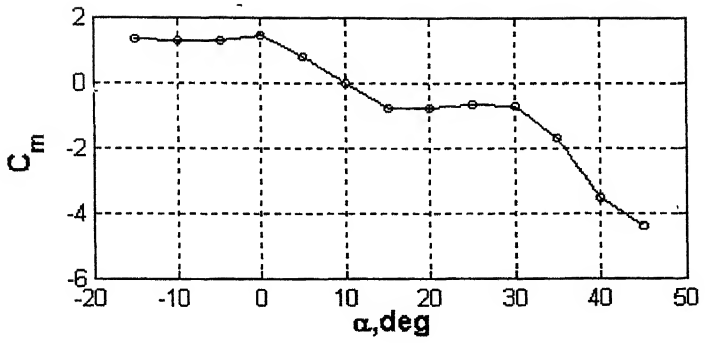

Fig. 2.4.9 Pitching Moment coefficient for body and fin at cant = -10 deg.

Figure 2.4.9 shows C_m Vs α for δ = -10° .It is noted from the figure that missile is neutrally stable in the range of 15° < α < 30°. For α = 10° δ = -10°, one would expect to measure C_m equal to values of body alone, if the fin experienced no normal force. But as pointed out earlier, the shed vortex flow from body seems to give rise to normal force on fins and this in turn, will create a nose down C_m .As α increases ,the vortex flow at the corresponding α would pass over the fin increasing distance and less and less normal force would be induced. However, increase in α will increase the fin contribution of C_N due to increase in angle of attack seen by the fin. These two effects seem to add to increase C_N with α in such a way that the negative C_m produced is more in magnitude as compared to the positive C_m due to body in the α values varying between 15° to 30°. The difference in body and fin contributions remains a constant in the range of 15° < α < 30° and thus the observed neutral stability in this range of α. Also it is noted that at α=10°,the negative C_m due to fin and positive C_m due to body exactly cancel each other, providing the condition (C_m =0) for α = 10° and δ = -10° .Beyond 30°, again due to

drop off in body contribution, the overall C_m becomes increasingly negative with α and thus makes the missile stable.

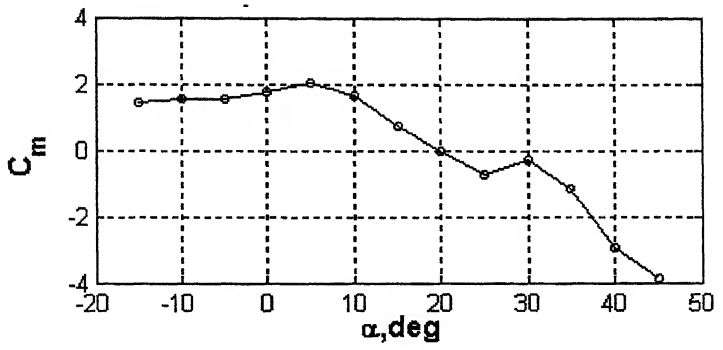

Fig. 2.4.10 Pitching Moment coefficient for body and fin at cant = -20deg.

For δ = -20°, -25° and –30°, the neutral stability is again observed but not so emphatically. For example, Fig. 2.4.10 for δ= -20° shows that C_m in the range of $20° < \alpha < 30°$ is changing from negative at α = 20° to positive at α = 25° and to negative again for α=30°. If fluctuations were assigned to experimental errors, and C_m value is averaged out for $20° < \alpha < 30°$, the C_m Vs α would again show neutral stability. Beyond, α=30°, as explained earlier, net C_m starts to build up to more and more negative values and missile is stable again. Also, as observed for α = 10° ,δ= -10° combination ,the α = 20° ,δ= -20° combination also shows trim condition (C_m =0) .

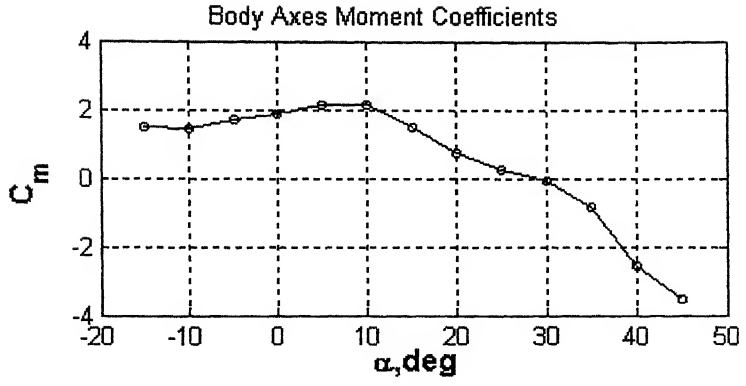

Fig. 2.4.11 Pitching Moment coefficient for body and fin at cant = -25deg.

A less than obvious similar trend can be observed by closely studying Fig. 2.4.11 that shows C_m Vs α for δ= -25°. Here again, for 25° < α < 30°, the C_m Vs α curve seems to relatively flatten out before again becoming negative for α >30°.Also it is noted that for α = 25°, δ = -25° combination, the trim condition (C_m =0) is achieved.

Finally, Fig. 2.4.12 shows results of C_m Vs α for δ= -30°.

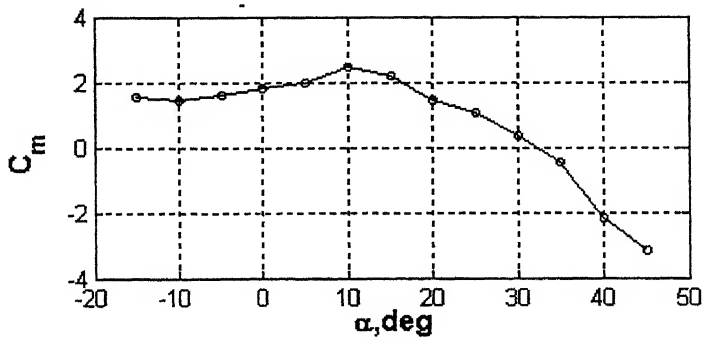

Fig. 2.4.12 Pitching Moment coefficient for body and fin at cant = -30deg.

Here one would expect no neutral stability as we are already at δ = -30° and for α>30°, the decreasing value of body C_m would not get cancelled by fin contribution and thus a negative $C_{m\alpha}$ is observed. Also, it is noted that unlike for other combinations of α = x°

,δ= -x° for α = 30° ,δ = -30° no trim (C_m = 0) is achieved , and a net small value of C_m is observed, and trim is observed at slightly high value of α = 32°

Trim of the Missile: As pointed out, it is worth emphasizing that the missile trim (C_m=0) is achieved at values α =-δ for all the settings of δ. Fig. 2.4.7- 2.4.12 discussed earlier show this for all the δ settings. One case of positive δ settings of 10° is given in Fig 2.4.13 Here again, it can be seem that the missile trims at α = -10°. This is a very important aspect of the design. The α_{trim} is achievable by simply deflecting the fins to the corresponding value of opposite sign.

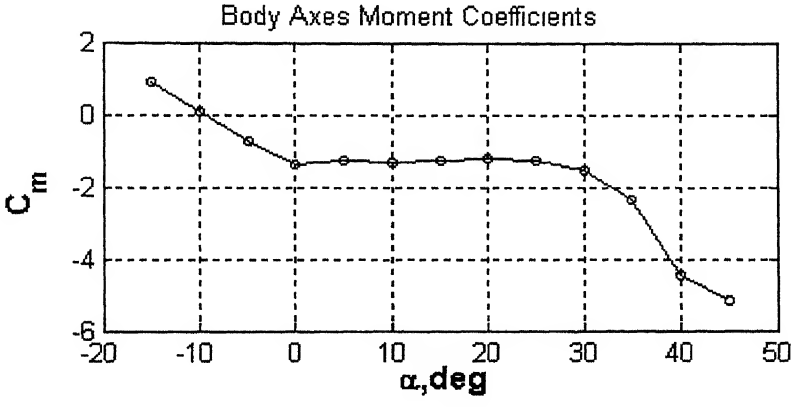

Fig. 2.4.13 Pitching Moment coefficient for body and fin at cant = +10deg

Conclusion: It appears to be a well-designed missile from operations point of view. It has neutral or low stability in the desired range of trim angle-of-attack range. For further understanding and appreciation of aerodynamic flow past the missile at varying α and δ, flow visualization test are planned in near future. Also to scan the data for varying α, a new model is being fabricated to meet stringent accuracy requirements and also enable the fin settings to be changed by remote control during the tests. The present model seemed to have slight curved fins and slight asymmetry in geometric shape.

FORCE COEFFICIENT C_Y

For body alone, referring to Fig 2.4.14 it can be seen that C_Y is close to zero for α up to 20^0. Since the model is symmetric and is not subjected to any sideslip angle, one should expect $C_Y = 0$ for all range of α under normal circumstances. However it can be seen from the Fig. 2.4.14, that C_Y abruptly becomes positive between $\alpha = 20^0$ to $\alpha = 40^0$. A positive C_Y should result in negative C_n. The wind tunnel data indeed show negative C_n for the range of $\alpha = 20^0$ to $\alpha = 40^0$. This is attributed to generation of asymmetric vortices at high angle of attack.

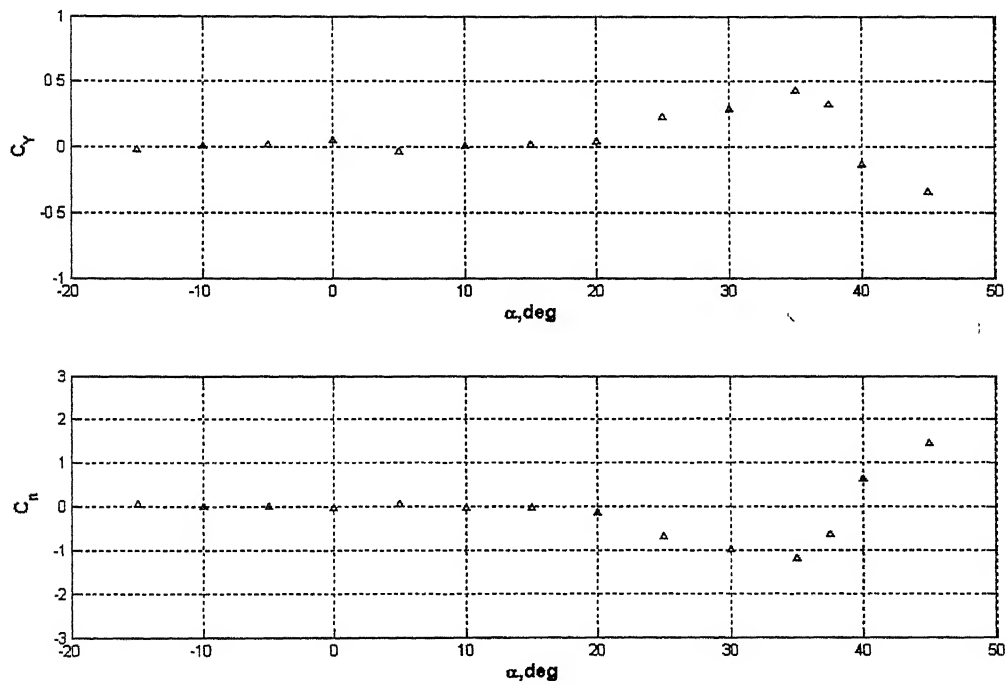

Fig 2.4.14 C_Y, C_n from Wind Tunnel as a function of angle of attack for body alone

2.4.2 THEORETICAL METHOD:

Theoretical methods explained in earlier section was applied to estimate force coefficient C_N and moment coefficient C_m. For body alone C_N and C_m were estimated for different values of angle-of-attack [-15° to 45°]. The results thus obtained were compared.

2.4.3 COMPARISION OF THEORETICAL ESTIMATES WITH WIND TUNNEL DATA

BODY ALONE

To start with, normal force coefficient C_N for body alone was computed using eq (2.2) and eq (2.3). Theoretical estimates of C_N along with corresponding wind tunnel estimates given in Fig. 2.4.15 and Table 2.4.1.

Table 2.4.1 Comparison of Normal Force coefficient from wind tunnel and theoretical estimates for body alone configuration

Alpha, Deg,	Theoretical	Wind Tunnel
-15	-1.0261	-0.97323
-10	-0.56284	-0.51578
-5	-0.21944	-0.25778
0	0	0.12023
5	0.21944	0.22187
10	0.56284	0.55578
15	1.0261	0.96654
20	1 6015	1.3659
25	2.2848	1.6143
30	3 0483	1.8262
35	2.5464	2.2399
40	3.0184	2.7712
45	3.4924	3 028

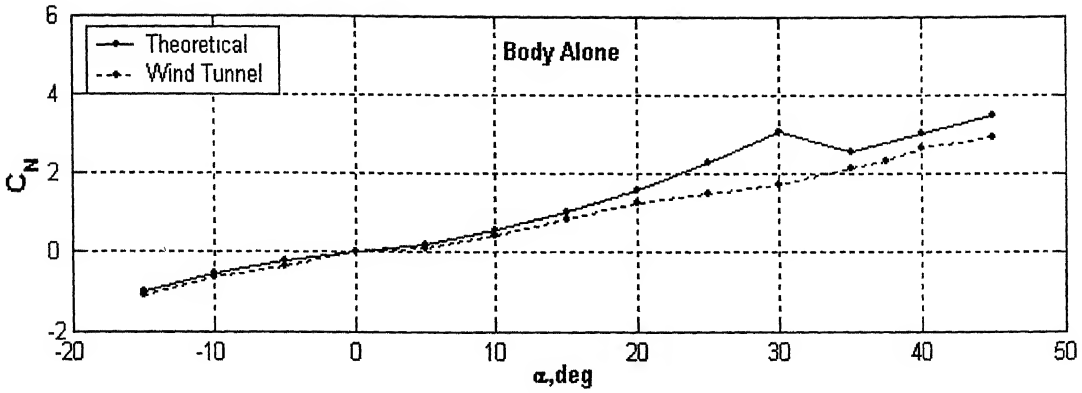

Fig 2.4.15 Comparison of Normal Force Coefficient from wind tunnel and theoretical estimates for body alone configuration.

Column (2) and Column (3) of table 2.4.1 lists the numerical values of body alone normal force coefficient C_N obtained through the theoretical and wind tunnel methods. It can be easily observed that within the α range of –15 to +15 deg, the estimated values of the coefficient compare well with the wind tunnel estimates. Beyond 20 deg., difference between the C_N estimated by the theoretical and wind tunnel method widens significantly, especially at angle of attack of 30 deg. This was expected as the theoretical methods (available /used) is not powerful enough to capture the effect due to asymmetric vortices at high angle of attack. Despite these limitations, in general theoretical prediction for the body alone is fairly good and can be used for initial design and analysis of the missile dynamics.

The fourth order equation for the fin alone normal force as given in equation (2.6) was used to compute C_N due to fin alone. In applying the fourth order equation, it was observed that addition of third form onwards yielded unrealistic value for $C_{N,fin}$ Since, angle of attack of interest was primarily up to 20-30 deg, it was decided to estimates $C_{N,fin}$ using first three terms of eq (2.6). Table (2.4.2) to (2.4.7) present tabular comparison between estimated value of C_N obtained through wind tunnel testing and theoretical method for different combination of angle of attack and tail setting angle. The values of C_N for different cant angles (-10 to –40) and angle of attack (-15 to 40) are compared graphically and presented through Fig (2.4.16) to (2.4.22).

Table 2.4.2 Comparison of wind tunnel and theoretical estimates for body and fin at cant=0° configuration

Alpha, Deg,	Theoretical	Wind Tunnel
-15	-1 5258	-1.2869
-10	-0.94077	-0.8899
-5	-0.4308	-0.49837
0	0	-0 098257
5	0.4308	0.40483
10	0 94077	0.82968
15	1.5181	1.3465
20	2.1564	2.0447
25	2.8571	2.1246
30	3.5927	2.4409
35	3.0105	3 204
40	3.3718	3.8027
45	3.7118	4.3538

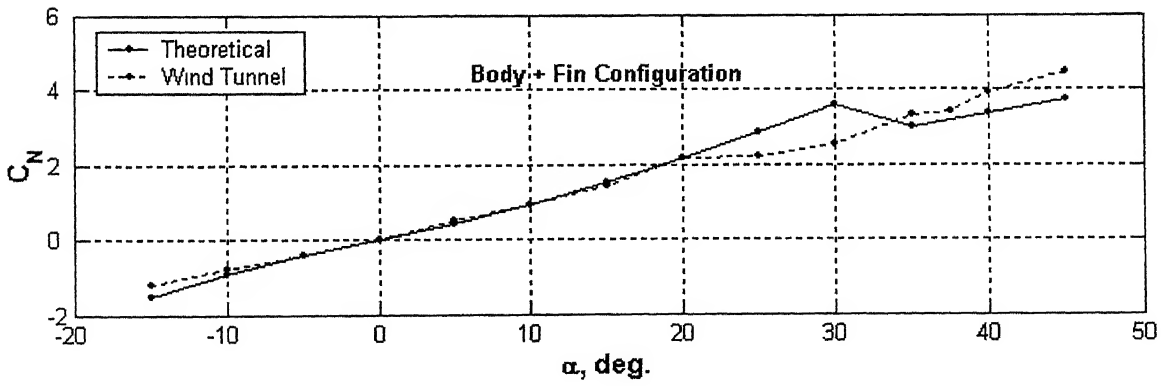

Fig 2.4.16 Comparison of wind tunnel and theoretical estimates for body and fin at cant=0° configuration.

Table 2.4.3 Comparison of wind tunnel and theoretical estimates for body and fin at cant=10 ^{0} configuration

Alpha, Deg,	Theoretical	Wind Tunnel
-15	-1.4397	-1.3803
-10	-0.56284	-0.80002
-5	-0 21019	-0.12293
0	0 19722	0.22698
5	0.55982	0.56841
10	1.0016	1.0792
15	1 5128	1.4198
20	2.0875	1.7351
25	2 7267	2.1161
30	3.404	2.5397
35	2 7736	2.923
40	3 0914	4.0674
45	3.3923	4.13

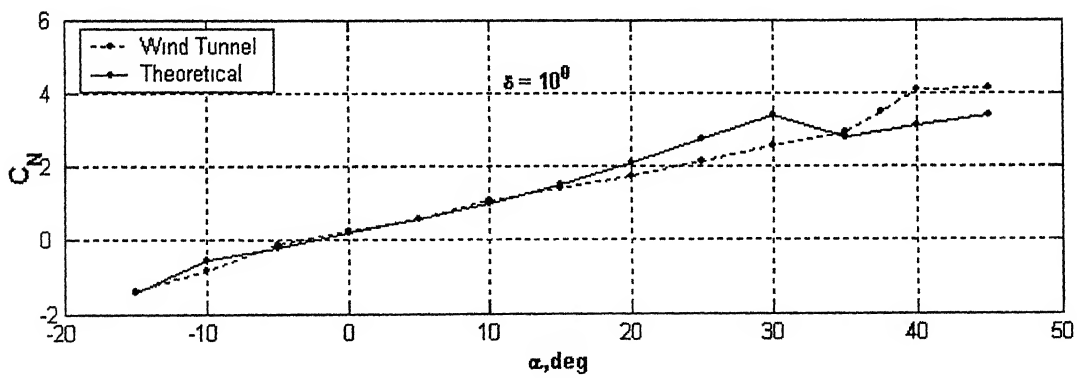

Fig 2.4.17 Comparison of wind tunnel and theoretical estimates for body and fin at cant=10 ^{0} configuration.

Table 2.4.3 Comparison of wind tunnel and theoretical estimates for body and fin at cant=-10 ^{0} configuration

Alpha, Deg,	Theoretical	Wind Tunnel
-15	-1.5184	-1.3801
-10	-1.0016	-0.97491
-5	-0.55982	-0.51546
0	-0.19722	-0.28287
5	0.21019	0.13138
10	0.56284	0.79674
15	1.4299	1.2271
20	2.1316	1.8027
25	2.8939	2.0677
30	3.6879	2.3512
35	3.1539	3.0214
40	3.5588	3.6635
45	3.9376	4.1373

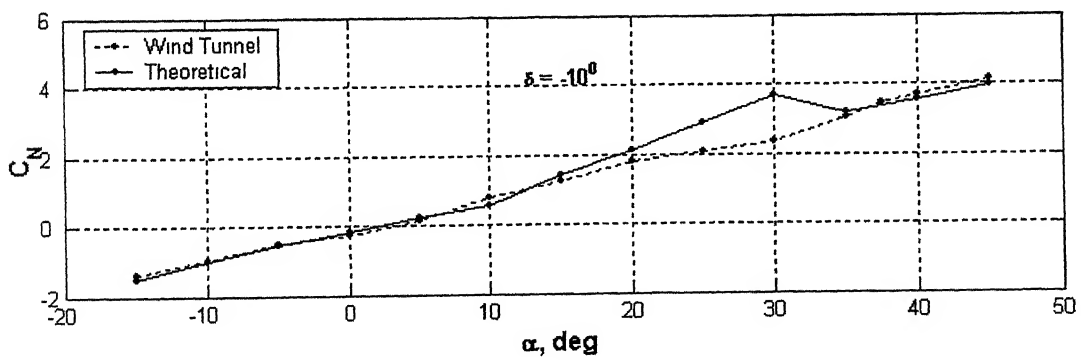

Fig 2.4.18 Comparison of wind tunnel and theoretical estimates for body and fin at cant=-10 ^{0} configuration.

Table 2.4.4 Comparison of wind tunnel and theoretical estimates for body and fin at cant=-20 ^{0} configuration

Alpha, Deg,	Theoretical	Wind Tunnel
-15	-1.4175	-0.5138
-10	-0.96884	-1.1263
-5	-0.59529	-0.63006
0	-0.30089	-0.42935
5	0.038321	-0.050532
10	0.54633	0.3504
15	1.2093	0.91168
20	1.6015	1.6051
25	2.8372	2.1897
30	3.6895	2.3456
35	3.2037	2.8375
40	3.6521	3.5549
45	4.07	3.8933

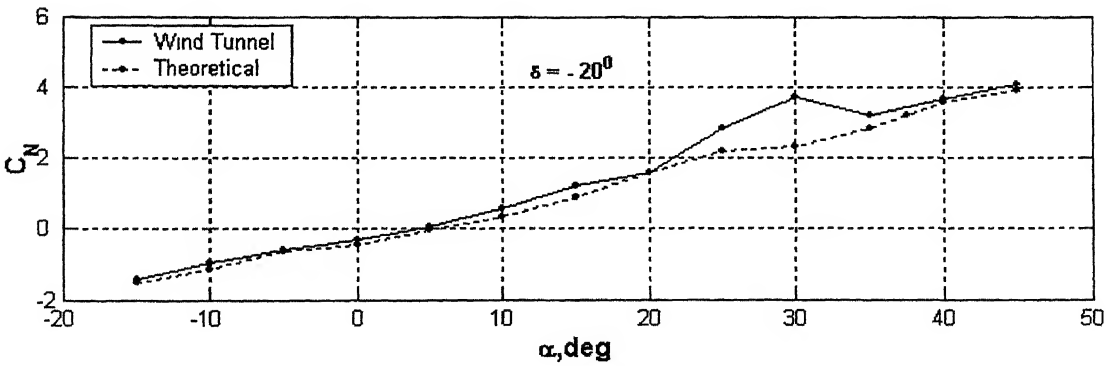

Fig 2.4.19 Comparison of wind tunnel and theoretical estimates for body and fin at cant=-20 ^{0} configuration

Table 2.4.5 Comparison of wind tunnel and theoretical estimates for body and fin at cant=-25 ^{0} configuration.

Alpha, Deg,	Theoretical	Wind Tunnel
-15	-1.3319	-0.4188
-10	-0.91739	-0.95947
-5	-0.57794	-0.65197
0	-0.31764	-0.51553
5	-0.012534	-0.14534
10	0.46137	0.19124
15	1.0912	0.82426
20	1.8636	1.5672
25	2.2848	1 756
30	3.6552	2.3354
35	3.1935	2.676
40	3.6637	3.3903
45	4.1011	3.8527

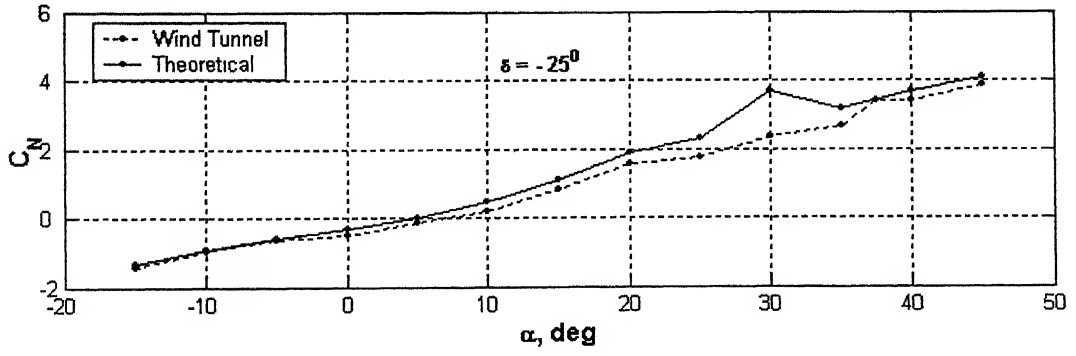

Fig 2.4.20 Comparison of wind tunnel and theoretical estimates for body and fin at cant=-25^0 configuration.

and fin at cant=-30 ^{0} configuration.

Alpha, Deg,	Theoretical	Wind Tunnel
-15	-1 223	-1 4489
-10	-0 84255	-0.9031
-5	-0.53721	-0.60135
0	-0.31101	-0.47117
5	-0.040001	-0 15712
10	0.3998	0.15578
15	0 9966	0.48343
20	1.7372	1.1881
25	2.6166	1.5794
30	3 0483	2 2049
35	3 1599	2.5196
40	3.652	3 2656
45	4 1088	3 9314

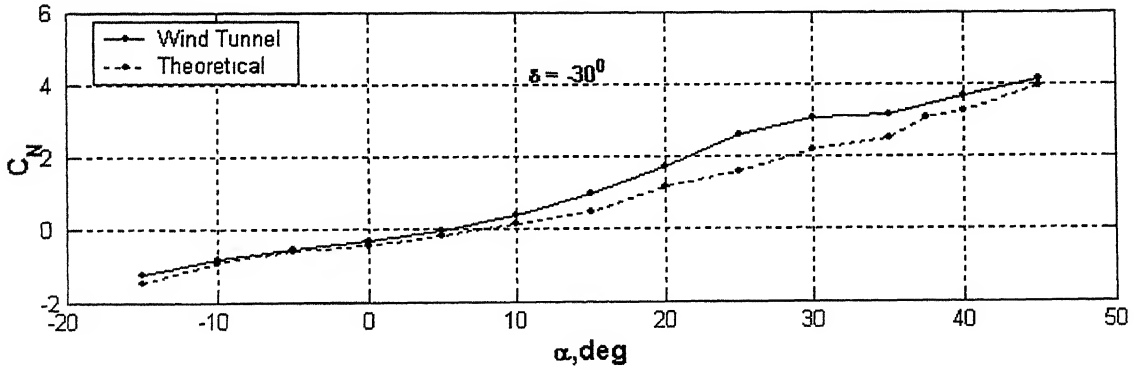

Fig 2.4.21 Comparison of wind tunnel and theoretical estimates for body and fin at cant=-30 ^{0} configuration.

Table 2.4.7 Comparison of wind tunnel and theoretical estimates for body and fin at cant=-35 ^{0} configuration.

Alpha, Deg,	Theoretical	Wind Tunnel
-15	-1.0906	-1.4313
-10	-0.74433	-1.0391
-5	-0.47308	-0.8554
0	-0.28099	-0.4415
5	-0 044081	-0 18083
10	0.36162	0.04584
15	0.92535	0.6772
20	1 6342	0.90318
25	2.4828	1.423
30	3.4346	1.9322
35	2.5464	2.3987
40	3.6168	3.1598
45	4 0931	3 5773

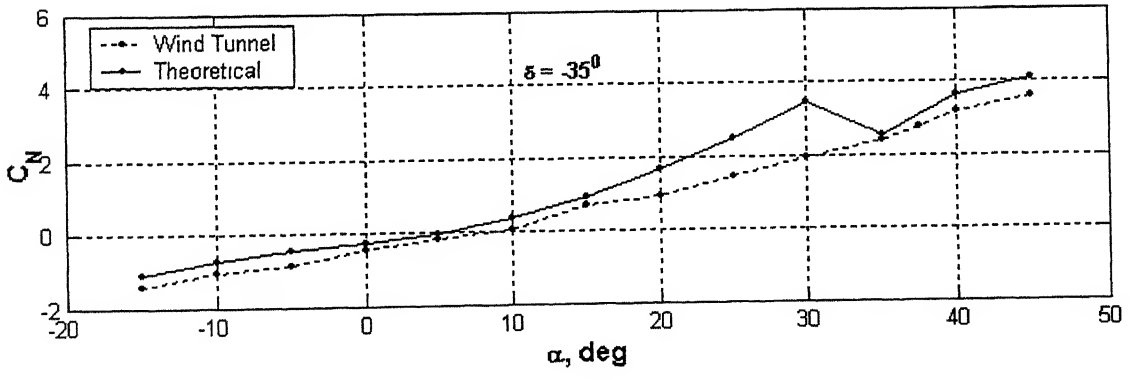

Fig 2.4.22 Comparison of wind tunnel and theoretical estimates for body and fin cant=-35 ^{0} configuration.

A closer look through these tables reveals that up to 15 deg, consistent matching exist with the wind tunnel estimates. In fact for =0 the matching between the both the estimates are fairly good. However the differences between theoretical and wind tunnel estimates widens up as tail angle is increased. In fact beyond angle of attack of 20 deg, where in fact asymmetric vortices have highly non-linear influence on fin performance, the prediction is poor. Even for small angle of attack as cant angle is increased the theoretical prediction shows large noticeable scatter from reference wind tunnel estimates.

Further it was also seen that for $\alpha = -\delta$, the theoretical predictions fail to capture the correct values of C_N and then C_m also. This is well understandable, as the method used here cannot take into account of effect of symmetric shedding vortices generated by the body on fin in estimation of normal force.

PITCHING MOMENT COMPARISION

Figure 2.4.23, Fig 2.4.24 graphically compares the values of pitching moment coefficients as obtained from theoretical methods and wind tunnel testing for a body alone configuration and for body and fin at a cant angle setting of zero deg. The comparison of C_m for body alone is presented in Fig 2.4.23 .It can be observed that theoretically estimated C_m does not compare well with the measured C_m. This is attributed to incorrect estimation of center of pressure by theoretical methods. Similar trend was observed while comparing estimated and measured C_m for body and fin at zero setting angle. This is pictorially presented in Fig. 2.4.24.Therefore, the center of pressure

as obtained from the wind tunnel estimates was used for calculating the theoretical C_m and it showed a close proximity with the measured C_m as shown in the figure; designated with * mark.

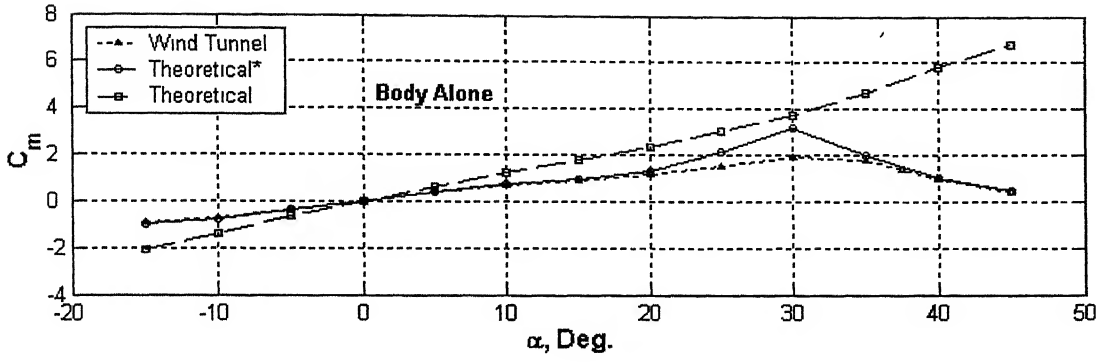

Fig 2.4.23 Comparison of Theoretical Estimates with Wind Tunnel for body alone.

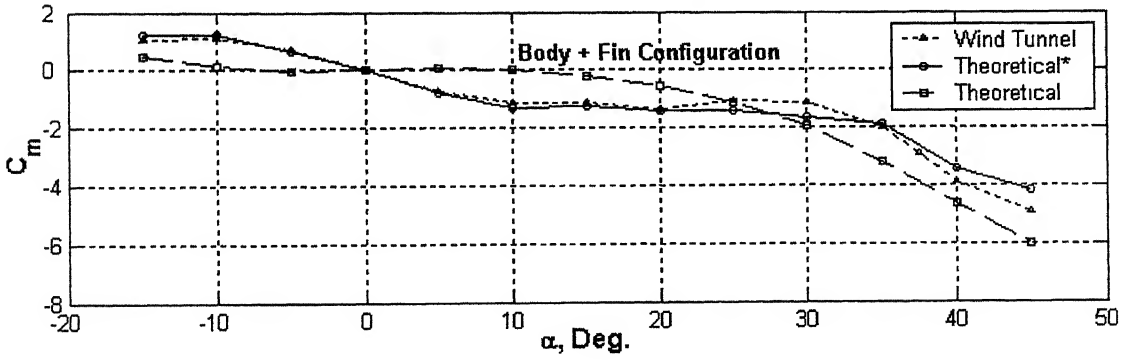

Fig 2.4.24 Comparison of Theoretical Estimates with Wind Tunnel for body and fin at cant=0 configuration.

*** - Center of pressure obtained from wind tunnel used.**

Chapter 3

TRAJECTORY MODELLING AND DEVELOPMENT OF CONTROL INPUT STRATEGY

3.1 GENERAL

The six degrees of freedom model is the ultimate in trajectory models allowing missile to have yaw in two planes as well as three spatial degrees of freedom and spin. It is not necessary to make any assumption regarding the linearised aerodynamics and the results obtained from the model would be exact. However the in determinability of many of the initial conditions and aerodynamic coefficients which are required as input frequently results in model not giving significantly good results. Nevertheless it is powerful tool for an ammunition designer.

3.2 DEVELOPMENT OF SIX DEGREES OF FREEDOM TRAJECTORY MODELLING

The six degrees of freedom model is based on the basic Newton laws which state that summation of all external forces in any direction must be equal to the time rate of change of momentum and the summation of all the moments of external forces must be equal to the time rate of change of angular momentum, all measured with respect to axis fixed in space. This can be stated mathematically as

$$\sum F_x = m.a_x \tag{3.1}$$

$$\sum F_y = m.a_y \tag{3.2}$$

$$\sum F_z = m.a_z \tag{3.3}$$

$$\sum L = \frac{dH_x}{dt} \tag{3.4}$$

$$\sum M = \frac{dH_y}{dt} \tag{3.5}$$

$$\sum N = \frac{dH_z}{dt} \tag{3.6}$$

The angular momentum vector can be represented as

$$H = \begin{pmatrix} I_{xx} & -I_{xy} & -I_{xz} \\ -I_{xy} & I_{yy} & -I_{yz} \\ -I_{xz} & -I_{yz} & I_{zz} \end{pmatrix} .\omega \tag{3.7}$$

The components of ω are p,q,r in the body axes system by definition and thus can be written as

$$\omega = p\bar{i} + q\bar{j} + r\bar{k} \tag{3.8}$$

With the above substitutions the forces and moment equations can be written as

$$F_x = m(\dot{u} + qw - rv) \tag{3.9}$$

$$F_y = m(\dot{v} + ru - pw) \tag{3.10}$$

$$F_z = m(\dot{w} + pv - qu) \tag{3.11}$$

$$M_x = \dot{p}I_{xx} - \dot{q}I_{xy} - \dot{r}I_{xz} + qr(I_{zz} - I_{yy}) + (r^2 - q^2)I_{yz} - pqI_{xz} + rpI_{xy} \tag{3.12}$$

$$M_y = -\dot{p}I_{xy} + \dot{q}I_{yy} - \dot{r}I_{yz} + rp(I_{xx} - I_{zz}) + (p^2 - r^2)I_{xz} - qrI_{xy} + pqI_{yz} \tag{3.13}$$

$$M_z = -\dot{p}I_{xz} + \dot{q}I_{yz} + \dot{r}I_{zz} + pq(I_{yy} - I_{xx}) + (q^2 - p^2)I_{xy} - rpI_{yz} + qrI_{xz} \tag{3.14}$$

3.2.1 EXTERNAL FORCES

The external forces F_x, F_y, F_z can be written as

$$F_x = F_{x,aero} + F_{x,grav} + F_{x,Thrust} \tag{3.15}$$

$$F_y = F_{y,aero} + F_{y,grav} \tag{3.16}$$

$$F_z = F_{z,aero} + F_{z,grav} \tag{3.17}$$

$$F_{x,aero} = \overline{q}SC_x \tag{3.18}$$

$$F_{y,aero} = \overline{q}SC_y \tag{3.19}$$

$$F_{z,aero} = \overline{q}SC_z \tag{3.20}$$

$$F_{x,grav} = -mg\sin\theta \tag{3.21}$$

$$F_{y,grav} = mg\cos\theta\sin\phi \tag{3.22}$$

$$F_{z,grav} = mg\cos\theta\cos\phi \tag{3.23}$$

The external force equation can now be collectively written as

$$F_x = \overline{q}SC_x - mg\sin\theta + T \tag{3.24}$$

$$F_y = \overline{q}SC_y + mg\cos\theta\sin\phi \tag{3.25}$$

$$F_z = \overline{q}SC_z + mg\cos\theta\cos\phi \tag{3.26}$$

3.2.2 EXTERNAL MOMENTS

The external moments M_x, M_y, M_z can be written as

$$M_x = \overline{q}SbC_l \tag{3.27}$$

$$M_y = \overline{q}SbC_m \tag{3.28}$$

$$M_z = \overline{q}SbC_n \tag{3.29}$$

It should be noted that the external forces and moments are w.r.t the inertial frame of reference i.e. Earth fix axes while the momentum and angular momentum terms are w.r.t body axes system. Thus suitable transformations of body fixed axes system to earth

fix axes system is necessary as the Newton mechanics is valid for inertial frame of reference only. The Euler angles θ,ϕ,ψ define the transformations that transform earth fix axes to body axes at any particular instant of time. The transformation is obtained by rotation of body axes, the order of rotation in which is very important.

$$V_{earth\ fixed} = \begin{pmatrix} \cos\psi & -\sin\psi & 0 \\ \sin\psi & \sin\psi & 0 \\ 0 & 0 & 1 \end{pmatrix} \begin{pmatrix} \cos\theta & 0 & \sin\theta \\ 0 & 1 & 0 \\ -\sin\theta & - & \cos\theta \end{pmatrix} \begin{pmatrix} 1 & 0 & 0 \\ 0 & \cos\phi & -\sin\phi \\ 0 & \sin\phi & \cos\phi \end{pmatrix} .V_{body\ fixed} \tag{3.30}$$

$$\dot{\phi} = p + q\tan\theta\sin\phi + r\tan\theta\cos\phi \tag{3.31}$$

$$\dot{\theta} = q\cos\phi - r\sin\phi \tag{3.32}$$

$$\dot{\psi} = r\cos\phi\sec\theta + q\sin\phi\sec\theta \tag{3.33}$$

The equations used to transform the body-axis velocity (u, v, w) into earth fixed axis are:

$$\dot{X} = u\cos\psi\cos\theta + v\left(\cos\psi\sin\theta\sin\phi - \sin\psi\cos\phi\right) + w\left(\cos\psi\sin\theta\cos\phi + \sin\psi\sin\phi\right) \tag{3.34}$$

$$\dot{Y} = u\sin\psi\cos\theta + v\left(\sin\psi\sin\theta\sin\phi + \cos\psi\cos\phi\right) + w\left(\sin\psi\sin\theta\cos\phi - \cos\psi\sin\phi\right) \tag{3.35}$$

$$\dot{Z} = u\sin\theta - v\cos\theta\sin\phi - w\cos\theta\cos\phi \tag{3.36}$$

3.2.3 WIND MODELLING

The wind components of velocity are also taken into account by appropriate wind modelling.

$$u' = u - W_x \cos\theta \cos\psi + W_y \cos\theta \sin\psi + W_x \sin\theta \tag{3.37}$$

$$v' = v - W_x \left(\cos\psi \sin\theta \sin\phi - \sin\psi \cos\phi\right) - W_y \left(\cos\psi \cos\phi + \sin\psi \sin\theta \sin\phi\right) + W_z \cos\theta \sin\phi \tag{3.38}$$

$$w' = w - W_x \left(\cos\psi \sin\theta \cos\phi + \sin\psi \sin\phi\right) - W_y \left(\sin\psi \sin\theta \cos\phi - \cos\psi \sin\phi\right) + W_z \cos\theta \cos\phi \tag{3.39}$$

The wind relative angle of attack and sideslip angles are computed using

$$\alpha = \tan^{-1} \frac{w'}{u'} \tag{3.40}$$

$$\beta = \tan^{-1} \frac{v'}{u'} \tag{3.41}$$

3.2.4 STANDARD ATMOSPHERE MODELLING

The International Civil Aviation Organization (ICAO) atmosphere, which is the most commonly used by aero ballisticians today is considered in the trajectory modelling in order to estimate the density and temperature variations with altitude. The ICAO standard atmosphere gives values of temperature and pressure and density up to an altitude of 20 km. It assumes sea level temperature of 15 ^{0} C and a pressure of 101.325 mbars and density of 1.225 kg/m^3. The variation of density and velocity of sound are modeled using the following.

$$\rho = 1.225(1 - 0.000022557695.Z)^{4.25587} \tag{3.42}$$

$$V_{sound} = 340.249(\frac{288.15 - 0.0065.Z}{288.15})^{0.5} \tag{3.43}$$

3.2.5 AERODYNAMIC MODEL FOR SIX DEGREE OF FREEDOM MODEL

$$C_N = C_{N\alpha}.\alpha + C_{N\delta}.\delta + C_{Nq}.\frac{qd}{2v} \tag{3.44}$$

$$C_A = C_{A\alpha}.\alpha + C_{A\delta}.\delta + C_{Aq}.\frac{qd}{2v} \tag{3.45}$$

$$C_m = C_{m\alpha}.\alpha + C_{m\delta}.\delta + C_{mq}.\frac{qd}{2v} \tag{3.46}$$

$$C_Y = C_{y\beta}.\beta + C_{y\delta a}.\delta a + C_{yp}.\frac{pd}{2v} + C_{yr}.\frac{rd}{2v} + C_{y\delta r}.\delta r \tag{3.47}$$

$$C_l = C_{l\beta}.\beta + C_{l\delta a}.\delta a + C_{lp}.\frac{pd}{2v} + C_{lr}.\frac{rd}{2v} + C_{l\delta r}.\delta r \tag{3.48}$$

$$C_n = C_{n\beta}.\beta + C_{nr}.\frac{rd}{2v} + C_{n\delta a}.\delta a + C_{np}.\frac{pd}{2v} + C_{n\delta r}.\delta r \tag{3.49}$$

Once the coefficients $C_N, C_Y, C_X, C_m, C_n, C_l$ are suitably modeled then the six-degree of freedom model equations serves as a fairly accurate tool for trajectory modeling.

3.3 DEVELOPMENT OF CONTROL INPUT STRATEGY FOR MISSION REQUIREMENT

The mission requires that the missile should have a leveled flight at height of approximately 500 meters. Thus development of control input strategy through the fins so as to obtain the desired trajectory was an important step in the trajectory modeling of the

missile. By control input strategy we mean, that for the desired flight path what should be the deflections given to the fins as a function of time. This strategy once developed can be used to pre-program the fin deflection. In order to get the required fin deflections, the trajectory model was run for different sets of deflections. The trajectory was simulated with these deflections. The mission requirements were:

1.The missile should attain a maximum height of around 500 meters in shortest possible time.

2.After attainment of maximum height it should maintain a leveled flight up to the terminal phase.

By varying the time intervals and magnitude of fin deflections three sets of fin deflections were chosen .The angle of attack α, flight path angle γ, height etc were monitored. Thus by careful study of all the parameters the strategy was developed for the control deflection during unguided phase.

Also it was required that angle of attack fluctuations should be minimum and to achieve zero flight path angles while maintaining a level flight at maximum height. So these deflections were linearly varied w.r.t time and thus the deflections were trimmed so as to:

1) Maintain zero γ angle during the level flight.

2) Reduce the α fluctuations.

3.4 RESULTS AND DISCUSSIONS

The fin deflections were given as a function of time and are shown in Fig 3.4.1–Fig3.4.5 The five set of different fin deflections shows the systematic approach to freeze the fin deflection requirement. These sets are tabulated in Table 3.4.1

Table 3.4.1 Control deflections for different sets

S.No	**t1**	δ_1	**t2**	δ_2	**t3**	δ_3
Set I	$0<t<5$	-10	$5\le t<8$	+10	$8\le t<12.5$	-5
Set II	$0<t<6$	-8	$6\le t<9$	+8	$9\le t<12.5$	-3
Set III	$0<t<5$	-9	$5\le t<9$	+7	$9\le t<12.5$	-4
Set 1V	$0<t<6$	-8	$6\le t<9$	+8	$9\le t<12.5$	-3
Set V	$0<t<6$	-7	$6\le t<9$	+8	$9\le t<12.5$	-1

It should be noted that the fin deflections were given constant for Set I-Set III and linearly varied between the time intervals **t1-t2** and **t2-t3** in Set IV to Set V.

From Fig 3.4.1 it can be seen that a height to 500 m is not achieved. Also there are undesirable fluctuations in angle of attack, α. Thus another set of deflections was chosen so that it can reduce the maximum height attained by the missile. As we know that a negative fin deflection results in a pitch up moment so it was necessary to give a lesser fin deflection in t1 interval in Set I. Fig 3.4.2 indicates that the missile is able to follow the desired trajectory path but it's angle of attack fluctuation, is certainly not permissible. This pattern is also followed in Fig 3.4.3.The angle of attack, α fluctuations in all the above cases was due to the sudden change in deflections from negative to positive in zero time intervals. So it was necessary to apply the deflections gradually.

In Set IV & Set V fin deflections were applied gradually maintaining a linear variation from **t1** to **t2** .Fig 3.4.4 shows the trajectory parameters obtained as a result of Set IV deflections. It is clear that the angle of attack, α got reduced substantially however requirement of 500 m height is not achieved. Further it was necessary to reduce fin deflections (δ_1).

Set V gave quite a promising configuration as shown in Fig 3.4.5. These set of deflections were frozen during all coarse of the subsequent analysis in the trajectory modeling. The final pre-programmed fin deflection used for further analysis is

$\delta_1 = -7$ deg.

$\delta_2 = +8$ deg.

$\delta_3 = -1$ deg.

It can be seen that with this pre-programmed fin deflection, the mission requirement of reaching 500 m as well as having level flight at 500 m with reduced angle of attack oscillation is achieved.

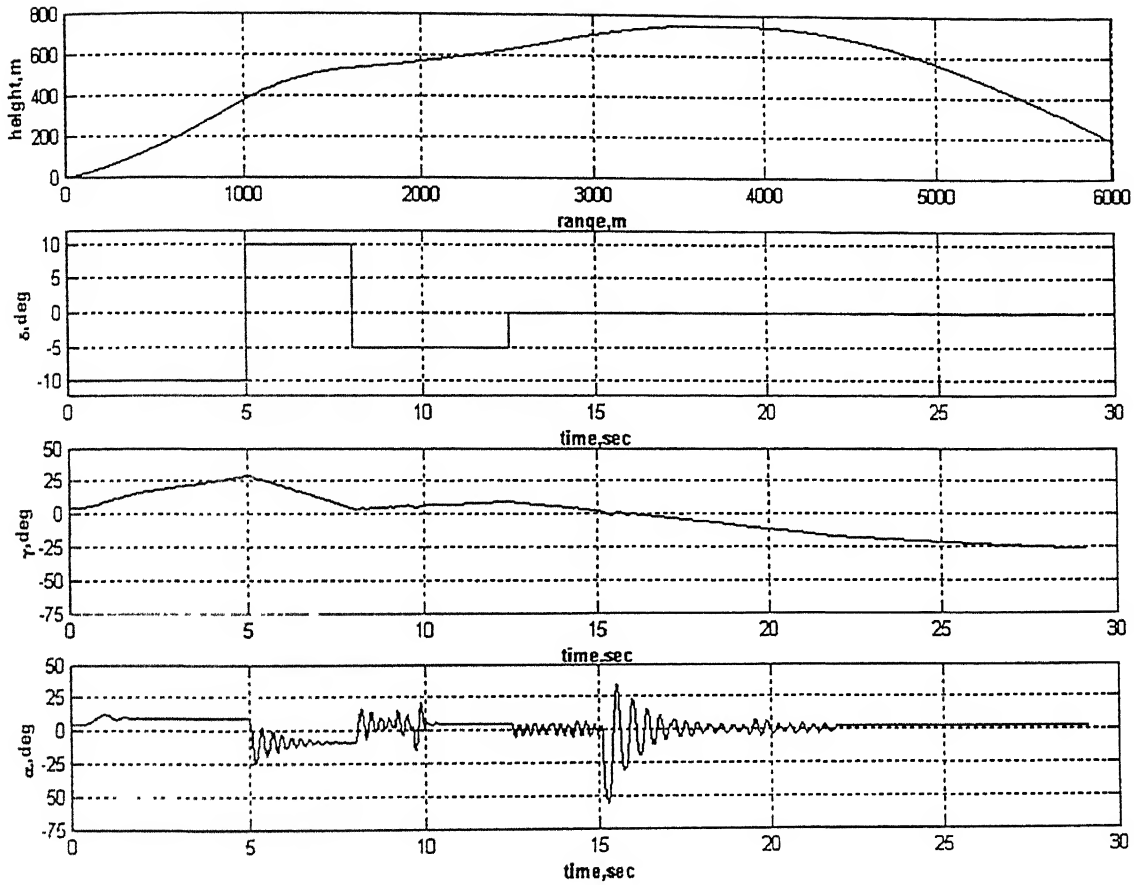

Fig 3.4.1 Time history of flight parameters with Set I deflections.

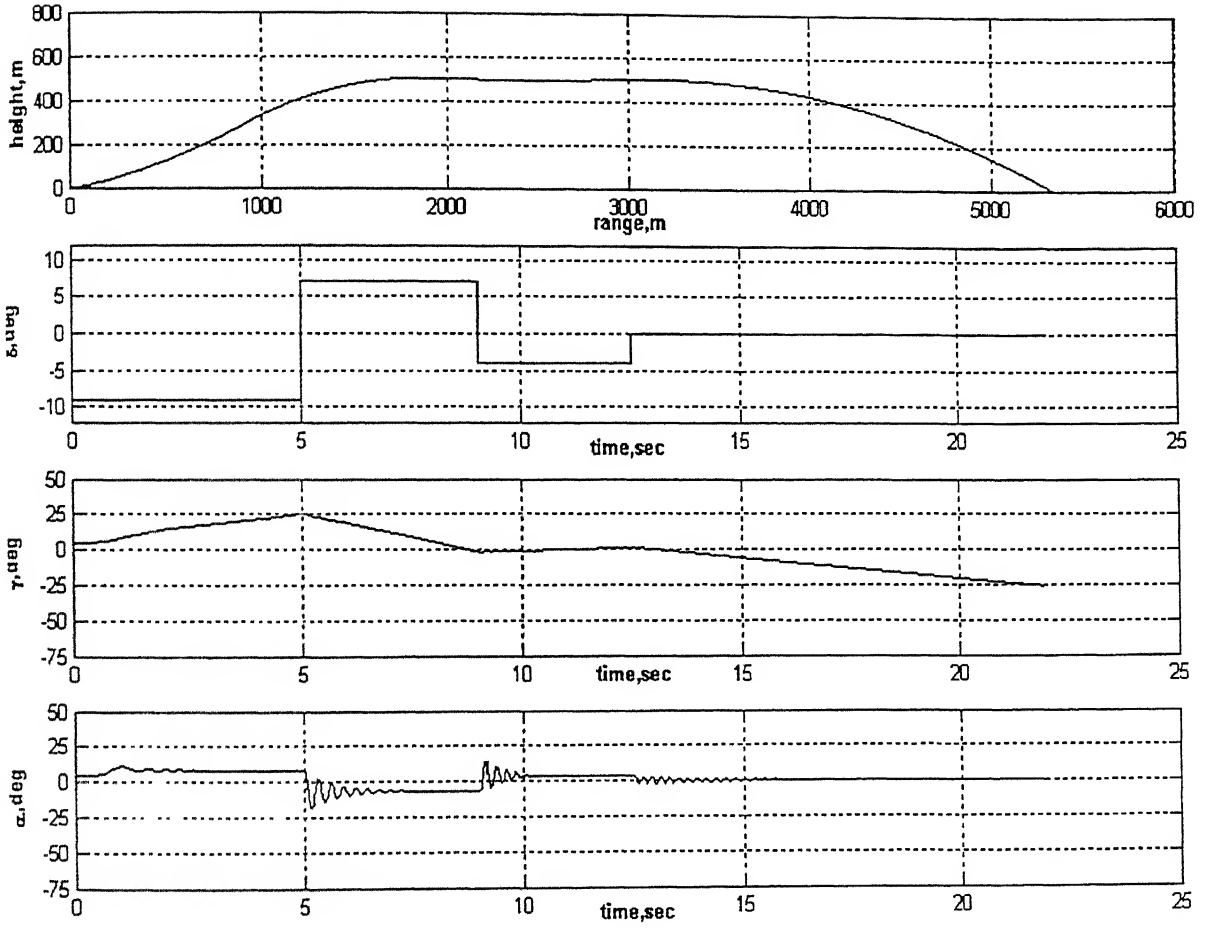

Fig 3.4.2 Time history of flight parameters with Set II deflections.

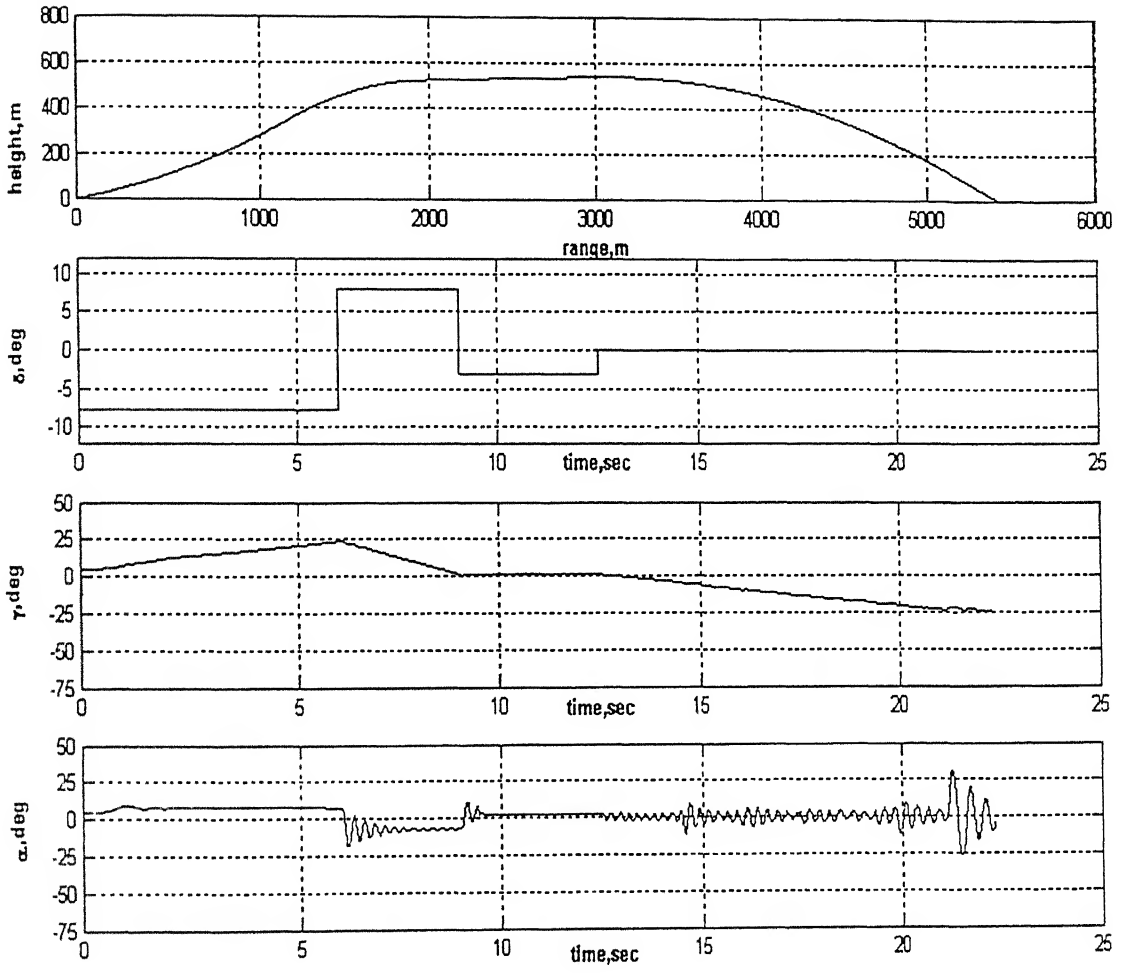

Fig 3.4.3 Time history of flight parameters with Set III deflections.

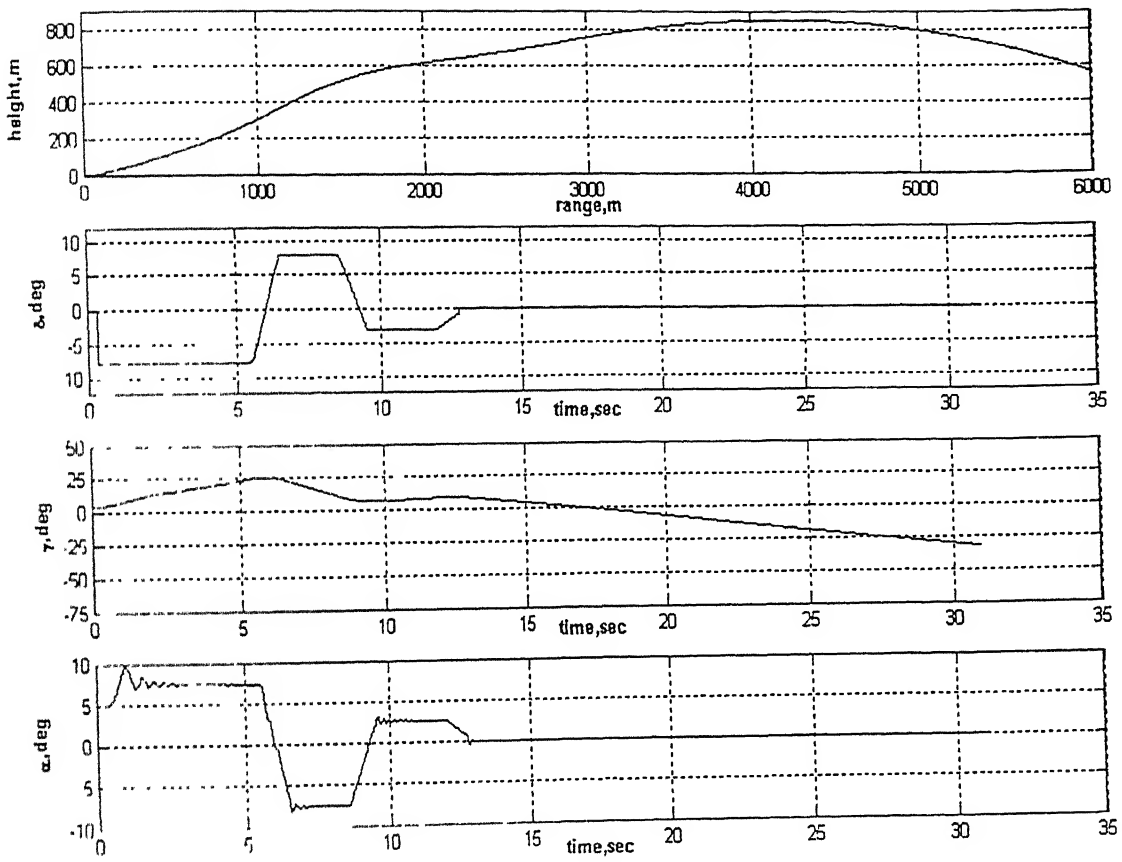

Fig 3.4.4 Time history of flight parameters with Set IV deflections.

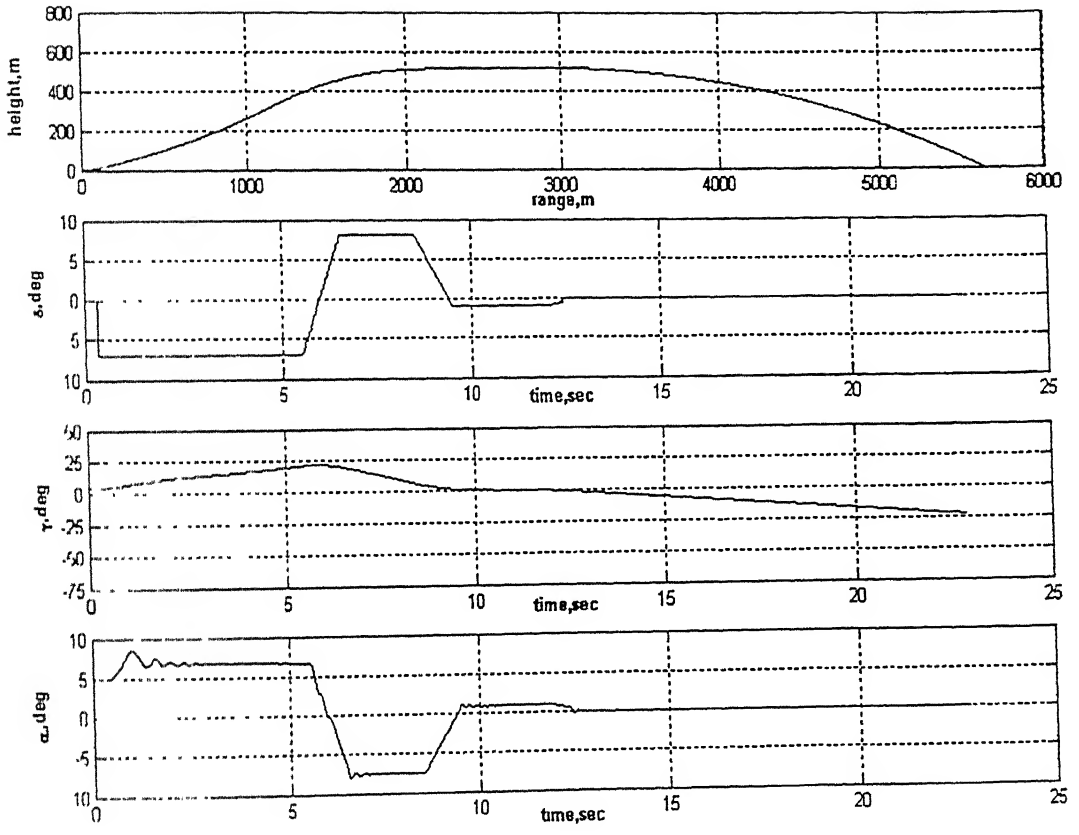

Fig 3.4.5 Time history of flight parameters with Set V deflections.

Chapter 4

TERMINAL GUIDANCE AND CONTROL REQUIREMENTS

4.1 GENERAL

Theoretically the proportional navigation law issues acceleration commands, perpendicular to the instantaneous missile target line of sight, which are proportional to the line of sight rate and closing velocity[14]. Mathematically, the guidance law can be stated as

$$a_c = N'.V_c.\dot{\lambda}$$

where a_c is the acceleration command, N' a unit less designer chosen gain (usually 3-5) known as the effective navigation ratio, V_c the missile target closing velocity and λ the line of sight angle (in radians). The over dot represents the time derivative of the line of sight angle or line of sight rate.

In tactical missiles, proportional navigation guidance commands are usually implemented by moving fins or other control surfaces to obtain the required acceleration.

4.2 SIMULATION OF PROPORTIONAL NAVIGATION IN TWO DIMENSION

As per the law of proportional navigation, the normal acceleration required to engage the target is given by

$$a_c = N'.V_c.\dot{\lambda} \tag{4.1}$$

$\dot{\lambda}$ is computed using the following relation

$$\dot{\lambda} = \frac{\bar{r} \times \bar{V}}{r^2} \tag{4.2}$$

where

$$\vec{r} = (x_T - x).\hat{i} + y.\hat{j}$$

$$\vec{V} = (\dot{x}_T - \dot{x}).\hat{i} + \dot{y}.\hat{j}$$

$\dot{\lambda}$ can be expressed explicitly as

$$\dot{\lambda} = \frac{-\dot{x}V_y + \dot{y}V_x}{x^2 + y^2} \tag{4.3}$$

V_c , the closing velocity is computed as

$$V_c = -\frac{d}{dt}\left[(x_T - x)^2 + y^2\right]$$

$$V_c = -\frac{\left[(x_T - x)(-\dot{x}) + \dot{y}\right]}{((x_T - x)^2 + y^2)^{1/2}} \tag{4.4}$$

The normal acceleration was then resolved along inertial x and y directions and solved for x, y to complete engagement simulation using following mathematical model.

$$\frac{d^2x}{dt^2} = -a_n \sin\lambda \tag{4.5}$$

$$\frac{d^2y}{dt^2} = a_n \cos\lambda \tag{4.6}$$

where

$$\frac{dx}{dt} = V_x = V\cos\gamma \tag{4.7}$$

$$\frac{dy}{dt} = V_y = V\sin\gamma \tag{4.8}$$

where γ is the flight path angle and a_c is computed using eq (4..1)

Initial conditions used for the simulations are

At $t = 0$, $x = x_0$ $y = y_0$

$$\dot{x} = \left(V \cos\theta\right)_{t=0}$$

$$\dot{y} = \left(V \sin\theta\right)_{t=0}$$

These equations were solved using fourth order runge kutta routine to arrive at missile trajectory

4.3 GENERATION OF REQUIRED NORMAL ACCELERATION

Based on kinematics analysis, it was found that to engage the target a definite value of normal acceleration (a_c), perpendicular to the line of sight, must be generated in flight. As stated earlier, this acceleration needs to be generated by the aerodynamic normal force acting on the missile. To ensure that sufficient acceleration is produced, a definite value of angle of attack must be introduced to the missile. The angle of attack is introduced by moving the tail in particular direction. The missile doesn't instantaneously respond to tail deflection as far as generating steady state acceleration is concerned. It takes definite time to build the trim angle of attack corresponding to a definite value of tail deflection. Since the missile is having low damping, it is must to device a stability augmentation system to artificially damp the oscillation so that steady state angle of attack, thus the acceleration is obtained almost instantaneously.

In this section, study has been carried out to model the dynamics including the expected value of trim angle of attack using non-linear aerodynamic model. Finally a tentative stability augmentation system has been proposed to enhance damping to obtain fast steady state response of the missile.

4.4 ESTIMATATION OF TRIM ANGLE OF ATTACK AND NORMAL ACCELERATION USING NON LINEAR MODEL

At trim angle of attack, net moment on the missile must be zero. The expression for moment coefficient for body fin with tail deflection is given by

$$C_m = (C_m)_{body,lin} + (C_m)_{body,nonlin} + (C_m)_{tail}$$

$$(C_m)_{body,lin} = \left[2.(k_2 - k_1) + \eta C d_c . \frac{A_p}{A_{ref}} . \sin^2 \alpha \right] \frac{(X_{cg} - X_{cp,body})}{d} \tag{4.9}$$

$$(C_m)_{tail} = [(C_{N\alpha})_{tail} (\alpha + \delta)] \frac{(X_{cg} - X_{cp,fin})}{d} \tag{4.10}$$

Following approximation was made to arrive at approximate analytic expression for trim angle of attack.

1. $\sin\alpha \approx \alpha$.

2.Centre of pressure of body and fin were assumed to be independent of angle of attack.

The moment coefficient C_m can be expressed as

$$C_m = Y_1.\alpha + Y_2.\alpha^2 + Y_3.\delta$$

$$Y_1 = (C_{N\alpha})_{body,lin} . \frac{(X_{cg} - X_{cp,body})}{d} + (C_{N\alpha})_{fin} . \frac{(X_{cg} - X_{cp,fin})}{d} \tag{4.11}$$

$$Y_2 = \eta C d_c . \frac{A_p}{A_{ref}} \frac{(X_{cg} - X_{cp,body})}{d} \tag{4.12}$$

$$Y_3 = (C_{N\alpha})_{fin} . \frac{(X_{cg} - X_{cp,fin})}{d} \tag{4.13}$$

At trim ,moment coefficient is zero, therefore, for a given fin deflection, δ, we get the equation for the trim angle of attack α_{trim} to be

$$0 = Y_1.\alpha_{trim} + Y_2.\alpha_{trim}{}^2 + Y_3.\delta \tag{4.15}$$

we can use quadratic formula to solve for the trim angle of attack. After eliminating the unrealistic root we get

$$\alpha_{trim} = \frac{-Y_1 - \sqrt{Y_1^2 - 4.Y_2 Y_3.\delta}}{2.Y_2} \tag{4.16}$$

The expression α_{trim} for different tail setting angle, δ has been used to compute steady state normal acceleration .It may be noted that at $|a_n| = |a_c|$ if $\theta = 0$,i.e. when missile aligns with the instantaneous line of sight.

$$a_n = \frac{\frac{1}{2}\rho V^2 S C_N}{m} \tag{4.17}$$

4.5 DESIGN OF STABILITY AUGMENTATION SYSTEM

Schematically the stability Augmentation system may be represented as follows:

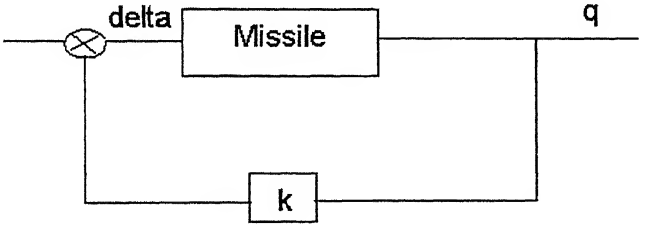

Fig 4.5.1 Schematic of a Stability Augmentation System (SAS)

The rate gyro flight control system artificially increases the low damping of the open loop flight control system by the use of rate gyro sensor and the principle of feedback. The tail deflection is proportional to the pitch rate to enhance pitch damping.

Pitch damping ratio, ξ and natural frequency ω_n obtained by pure pitching approximation [11] is:

$$\xi = \frac{-M_q}{2.\sqrt{-M_\alpha}} \tag{4.18}$$

$$\omega_n = \sqrt{-M_\alpha} \tag{4.19}$$

For short period approximation :

$$\xi = \frac{-(M_q + \frac{Z_\alpha}{V})}{2.\sqrt{M_q.\frac{Z_\alpha}{V} - M_\alpha}} \tag{4.20}$$

$$\omega_n = \sqrt{M_q.\frac{Z_\alpha}{V} - M_\alpha} \tag{4.21}$$

where

$$M_\alpha = \frac{\frac{1}{2}\rho V^2 S d C_{m\alpha}}{I_{yy}}$$

$$M_q = \frac{\frac{1}{2}\rho V^2 S d C_{mq}}{I_{yy}} . \left(\frac{d}{2V}\right)$$

$$Z_\alpha = \frac{-(C_{L\alpha} + C_{Do})\frac{1}{2}\rho V^2 S}{m}$$

Time to half amplitude and angle of attack response is computed using

$$T_{1/2} = \frac{0.693}{\xi.\omega_n} \tag{4.22}$$

$$\alpha(t) = \alpha_{trim} 1 + \frac{e^{-\xi\omega_n t}}{\sqrt{1-\xi^2}} \sin(\sqrt{1-\xi^2}\,\omega_n t + \varepsilon) \tag{4.23}$$

$$\alpha_{trim} = -\frac{M_{\delta e}.\delta_e}{M_\alpha} \tag{4.24}$$

$$\varepsilon = \tan^{-1}\frac{-\sqrt{1-\xi^2}}{-\xi} \tag{4.25}$$

For a pre-decided $T_{1/2}$ amplitude, ξ required is computed using expression for short period approximation as given in eq (4.22) & (4.20) respectively . In estimating ω_n using eq(4.21) , M_q is assigned zero value. Once ξ is known, for a given value of Z_α, M_α, V the required M_q value is estimated using eq (4.21). The derived M_q is attained artificially using ' q ' feedback to tail ($\Delta\delta_e = kq$).

Change in moment coefficient, ΔC_m, due to additional tail deflection is calculated using

$$\Delta C_m = C_{m\delta e}.\Delta\delta_e$$

Since $\Delta\delta_e = kq$

Thus the gain, k is estimated as

$$k = \frac{\left(C_{mq}\right)_{required} - \left(C_{mq}\right)_{basic}}{C_{m\delta e}} \cdot \frac{d}{2V} \tag{4.27}$$

The tail when deflected by kq, results in reduction in $T_{1/2}$ amplitude for a design value of ξ (required).

4.6 RESULTS AND DISCUSSION

4.6.1 TWO DIMENSIONAL TARGET ENGAGEMENT SIMUMATION-NORMAL ACCELERATION REQUIREMENT

For target engagement simulation, the target was assumed to be at 2000m.The missile was activated for guidance at a height of 500m as geometrically shown in Fig 4.6.1. Missile was fired at various angles ranging from $\theta = -20^{\circ}$ to $+30^{\circ}$ at a velocity 290 m/sec. Fig 4.6.2 pictorially presents target engagement simulation.

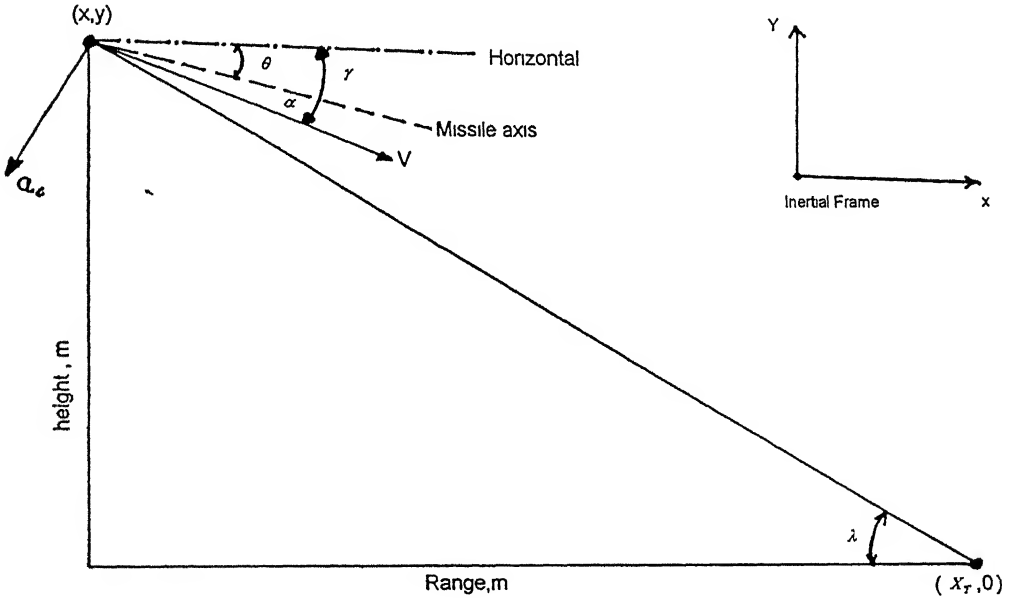

Fig 4.5.1 Two Dimensional Missile Target Engagement geometry

Target engagement simulation was carried at for various values of N' (3-5). It was found that for N' >= 3, the simulation results in exact matching. Though literature

recommends value of N' to be with in range of 3-5,however from the point of view of practical limitation, it is desirable to keep N'=3.

Results were generated for different angle of projection towards the target. The value of N'=3, ensures exact engagement of target for different angle of projection ($\theta = -20$ deg to +30 deg). This is pictorially presented in Fig. 4.6.2.however acceleration requirement for each case will be different for different values of initial launch angle, θ.It is obvious that for θ = 30 deg ,it will require largest normal acceleration to engage the target. In order to estimate the magnitude of normal acceleration (a_c), based on proportional navigation kinematics, the code was run at V=290 m/sec for different values of θ and a_c was recorded as presented in Fig. 4.6.3.It can also be seen that for θ=0, i.e. the missile fired horizontally, the a_c required is around 3g and for θ=-10 deg (relatively closer to the line of sight) the a_c required is around 1g.In practice ,since the missile is terminally guided , θ should be set close to line of sight with small leading angle, thus acceleration requirement can be reduced accordingly.

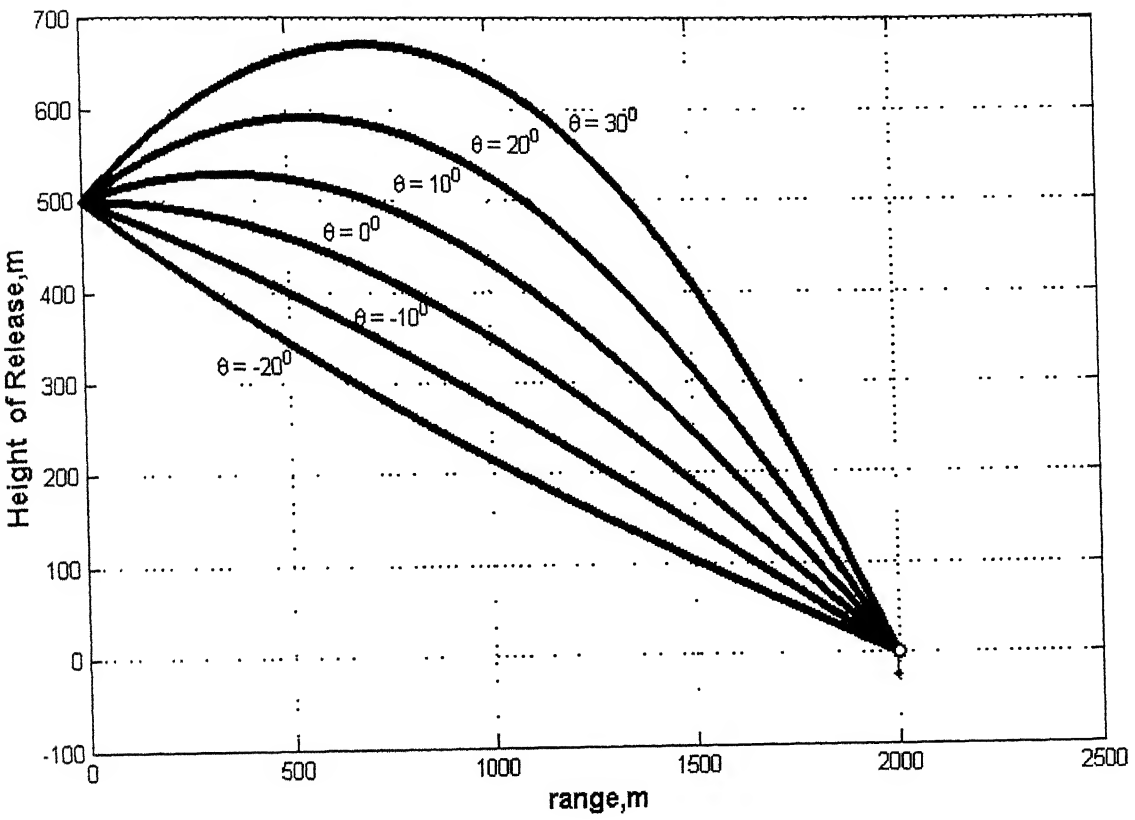

Fig 4.6.2 Two-dimensional missile target simulation

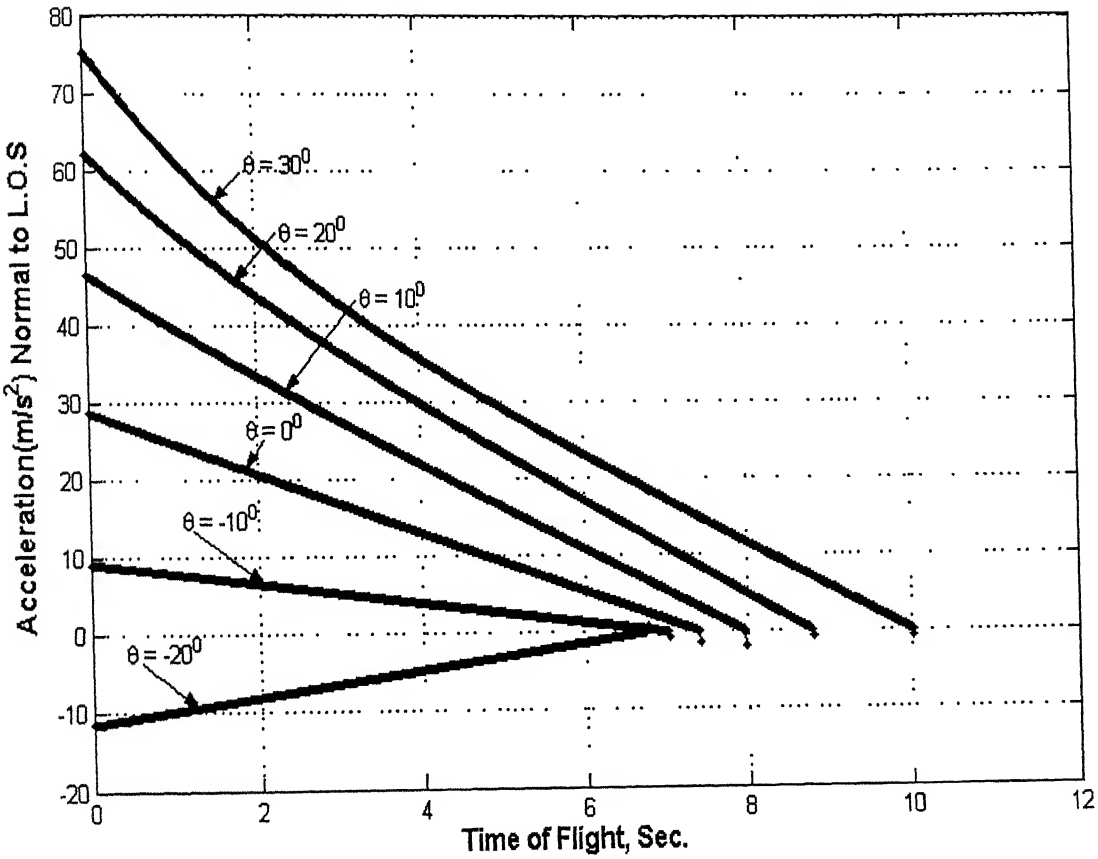

Fig 4.6.3 Variation of required acceleration normal to LOS for different release angle θ.

4.6.2 ESTIMATION OF TRIM ANGLE OF ATTACK AND NORMAL ACCELERATION

Trim angle of attack and normal acceleration are computed using eq (4.16) & (4.17). The values of trim angle of attack and normal acceleration a_n are computed for different tail setting angle and velocities. Table 4.6.1 presents the estimated values of trim angle of attack and normal acceleration for different setting angle and velocities. Figure 4.6.4 pictorially presents the result.

Table 4.6.1 Theoretical Estimation of α_{trim} & Normal acceleration a_n for different velocity and δ input.

δ, Deg.	Velocity	α_{trim}	a_n
5	200	-5.316	4.3294
5	230	-5.316	5.7256
5	260	-5.316	7.3166
5	280	-5.316	8.4855
5	290	-5.316	9.1025
10	200	-10.201	10.529
10	230	-10.201	13.925
10	260	-10.201	17.794
10	280	-10.201	20.637
10	290	-10.201	22.137
20	200	-19.012	26.733
20	230	-19.012	35.355
20	260	-19.012	45.179
20	280	-19.012	52.397
20	290	-19.012	56.207
25	200	-23.047	36.076
25	230	-23.047	47.711
25	260	-23.047	60.969
25	280	-23.047	70 709
25	290	-23.047	75.85
30	200	-26.883	45 912
30	230	-26.883	60 719
30	260	-26.883	77.592
30	280	-26.883	89.988
30	290	-26.883	96.531

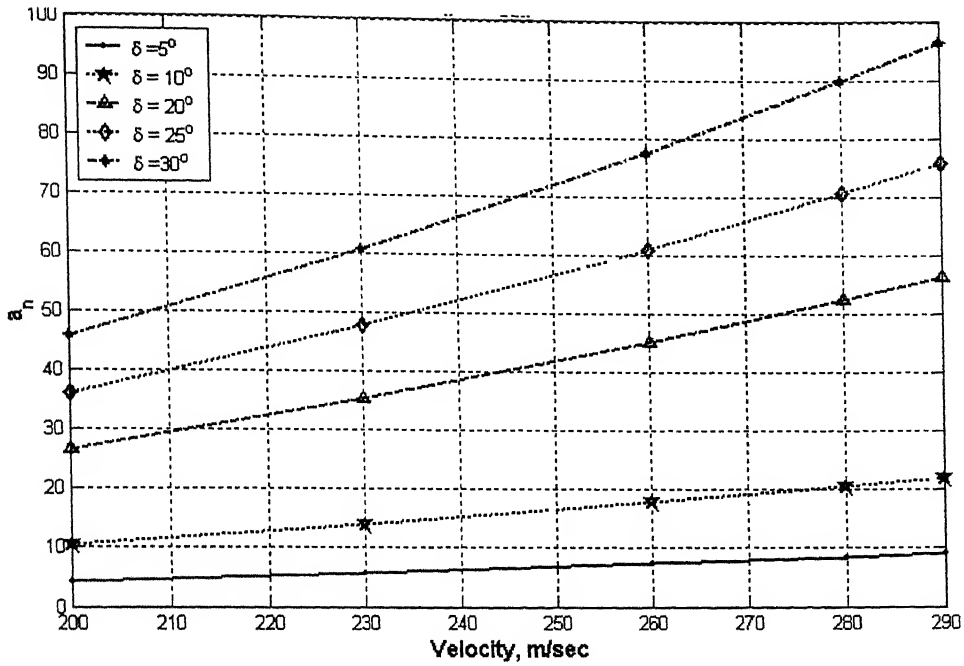

Fig 4.6.4 Variation of Theoretical a_n at α_{trim} for different fin deflection

Based on this study, it can be stated that to generate a 3g acceleration, the tail deflection of around 15 deg is required at a velocity of 290 m/sec.

4.6.3 DESIGN OF STABILITY AUGMENTATION SYSTEM (S.A.S)

To estimate the value of gain , k for updating pitch damping using pitch rate feedback the eq (4.27) has been used. $\left(C_{mq}\right)_{required}$ was calculated for a flight condition of velocity=290 m/sec at a height of 500 m. Table 4.6.2 lists the values of ξ required for different desired $T_{1/2}$ amplitude.

Table 4.6.2 Values of $T_{1/2}, \xi, k$ at Vel=290 m/sec and Height=500m

$T_{1/2}$ (sec)	ξ (Required)	k
0.1	0.427	0.04
0.05	0.854	0.08

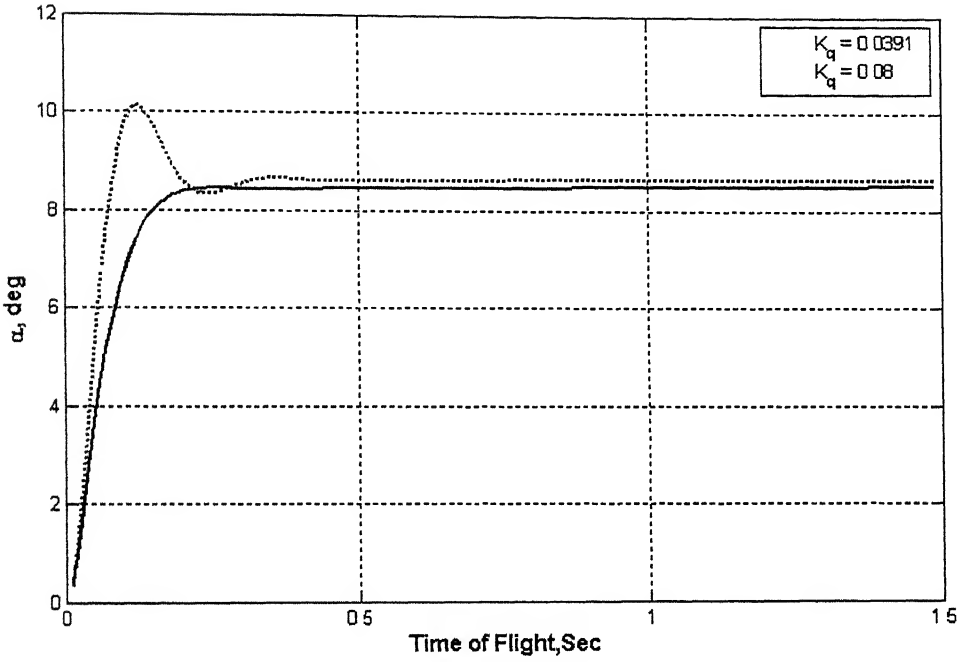

Fig 4.6.5 Variation of α damping for different SAS coefficient values.

For a specific case, as stated earlier $T_{1/2}$=0.1 sec is considered and the feedback gain k was estimated. Now six degree of freedom model was used to compute angle of attack time histories with and without feedback. For this specific case, the angle of attack response without feedback assumed zero pitch damping in open loop.

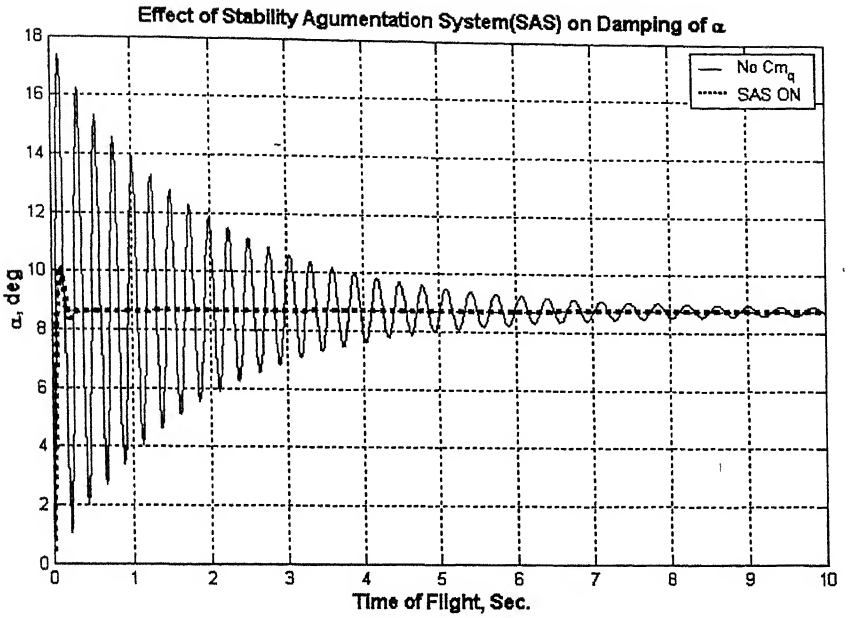

Fig 4.6.6 A comparative time history of α with and without feedback

A comparative time history of α with and without feedback is presented in Fig 4.6.6 .It can be easily verified that the steady state value reaches almost instantaneously. Thus it is validated that the scheme for stability augmentation system will enhance pitch damping to designed value.

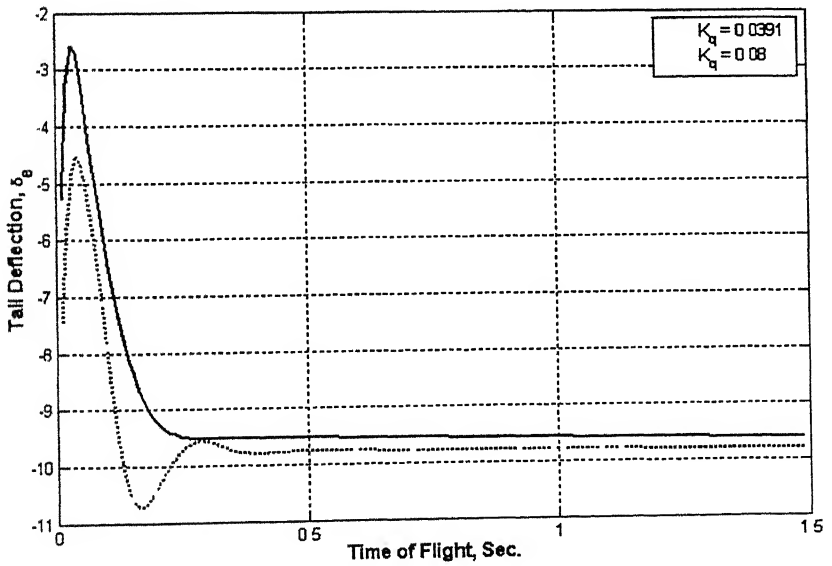

Fig 4.6.7 variation of fin deflection for different SAS coefficient values

CHAPTER 5

CONCLUSION AND SCOPE FOR FUTURE WORK

5.1 CONCLUSION

1. The task of generating aerodynamic parameters using theoretical wind tunnel methods have been completed. Based on the comparison it is observed that the functional form used in theoretical methods can be used to generate initial design parameters. The alteration of flow field due to shedding vortices could not be captured using theoretical methods, thus for fine tunning, wind tunnel estimates should be used.

2. Trajectory model has been developed to pre-program the tail deflection to satisfy the requirement of reaching height of 500 m and maintaining level flight up to 3000 m.

3. Normal acceleration (perpendicular to the line of sight) required to simulate target engagement has been modeled based on proportional navigation kinematics.

4. Missile response to generate the desired acceleration per unit tail deflection has been evaluated. Model to estimate expected steady state angle of attack (α_{trim}) has been proposed. In order to reduce the $T_{1/2}$ amplitude of missile airframe response, stability augmentation system has been proposed.

5.2 SCOPE FOR FUTURE WORK

1.Exhaustive wind tunnel testing for angle of attack sweep to fixed tail deflection should be carried out for fine-tuning.

2.Theoretical methods need to be updated to capture 'effect of shedding vortices' and the lifting characteristics of the missile.

3.Target engagement simulation using proportional navigation needs to be developed using six degree of freedom modeling.

REFERENCES

1. Kennedy , G.P. ,"Missiles and Spacecraft of National Air and Space Museum",Smithsonian Institution Press ,Washington DC,1983.

2. Benecke,T.,and Quick,A.W. ," History of German Guided Missile Development," Proceedings of AGARD first Guided Missile seminar,1956.

3. Nesline, F.W. , and Zurchan , P. , "A New Look at Classical Versus Modern Homing Guidance,"Journal of Guidance and Control., Vol.4,Jan-Feb,1981, pp.78-85.

4. Yuan , C.L. , "Homing and Navigation courses of Automatic Target-seeking Devices," RCA Labs.,Rept. PTR-12 C , Princeton , NJ,Dec 1942.

5. Benett , R.R. , and Mathews , W.E. , "Analytical Determination of Miss Distance for Linear Homing Navigation Ststems ," Huges Aircraft Co. ,TN-260 ,Culver city , CA,, March 1952.

6. Fossier , M.W. , "The Development of Radar Homing Missiles," Journal of Guidance Control , and Dynamics, Vol. 7 ,Nov-Dec. 1984,pp. 641-651.

7. Yuan, C.L.,"Homing and Navigation Courses of Automatic Target-seeking Devices," Journal of Applied Physics, Vol .19,Dec.1948 ,pp. 1122-1128.

8. Bryson, A.E., and Ho, Y.C., Applied optimal Control, 13 Laisdell, Waltham, MA, 1969.

9. Joset Rom , High angle of attack Aerodynamics , Subsonic ,Transonic and Super sonic Flows ,springer-verlag New York , Inc, 1992.

10. Moore , Frank .G. ,"Approximate Methods for Weapon Aerodynamics", Progress in Astronautics and Aeronautics, Apr 2000.

11. Maine, R.E., and Illiff, K.W. , "Application of Parameter Estimation to Aircraft Stability and Control," NASA RP 1168,1986.

12. The Engineering Design Handbook,"American Material Command, AMCP,706 -280.

13. Hoak , D.E. , USAF Stability and Control DATCOM; Air Force Flight Dynamics Laboratory,Wright Patterson Air force Base, Ohio,1960, revised 1975.

14. Zarchan, P.,"Tactical and Strategic Missile Guidance," 3 rd AIAA, Inc.1947.

APPENDIX 'A'

DATA BASE FOR ESTIMATION OF $(C_N)_{\alpha=15^0}$, $(C_N)_{\alpha=35^0}$ etc.

Table 2.2.1.(a) $(C_N)_{\alpha=15^0}$ as a function of Mach number, aspect ratio & taper ratio

Aspect ratio	Taper ratio	Mach number									
		0	0.6	0.8	1.0	1.2	1.6	2.0	3.0	4.5	≥6.0
≤0.5	0.0	0.28	0.29	0.30	0.32	0.33	0.33	0.32	0.24	0.175	0.125
	0.5	0.39	0.41	0.415	0.42	0.43	0.42	0.39	0.28	0.22	0.18
	1.0	0.34	0.34	0.36	0.40	0.42	0.42	0.40	0.30	0.23	0.19
1.0	0.0	0.43	0.44	0.46	0.49	0.53	0.47	0.43	0.33	0.26	0.21
	0.5	0.47	0.50	0.60	0.62	0.625	0.55	0.50	0.39	0.29	0.22
	1.0	0.46	0.48	0.52	0.58	0.60	0.55	0.51	0.39	0.29	0.22
2.0	0.0	0.55	0.59	0.65	0.67	0.68	0.58	0.48	0.33	0.26	0.22
	0.5	0.56	0.59	0.66	0.76	0.80	0.66	0.54	0.40	0.31	0.26
	1.0	0.56	0.59	0.66	0.76	0.70	0.62	0.55	0.38	0.29	0.23
≥4.0	0.0	0.65	0.66	0.71	0.83	0.86	0.73	0.59	0.43	0.31	0.23
	0.5	0.69	0.71	0.75	0.88	0.92	0.75	0.62	0.45	0.34	0.28
	1.0	0.69	0.71	0.75	0.88	0.92	0.75	0.62	0.45	0.34	0.28

$(C_N)_{\alpha=35^0}$ as a function of Mach number ,aspect ratio & taper ratio

Aspect ratio	Taper ratio	Mach number									
		0	0.6	0.8	1.0	1.2	1.6	2.0	3.0	4.5	≥6.0
≤0.5	0.0	0.89	0.91	0.93	0.95	0.98	0.95	0.88	0.72	0.65	0.61
	0.5	1.10	1.13	1.16	1.25	1.20	1.09	1.0	0.84	0.76	0.72
	1.0	1.06	1.08	1.13	1.16	1.19	1.12	1.03	0.86	0.76	0.72
1.0	0.0	1.18	1.20	1.22	1.24	1.18	1.09	1.0	0.80	0.70	0.66
	0.5	1.2	1.22	1.24	1.33	1.40	1.20	1.15	0.95	0.82	0.76
	1.0	1.10	1.11	1.16	1.26	1.36	1.20	1.16	0.95	0.82	0.76
2.0	0.0	0.95	1.01	1.13	1.20	1.28	1.18	1.08	0.93	0.86	0.81
	0.5	1.0	1.07	1.18	1.3	1.4	1.32	1.17	1.0	0.90	0.85
	1.0	0.98	1.05	1.17	1.27	1.39	1.32	1.21	1.0	0.90	0.85
≥4.0	0.0	0.97	1.05	1.17	1.21	1.34	1.22	1.10	0.95	0.87	0.83
	0.5	1.03	1.09	1.22	1.32	1.44	1.35	1.25	1.05	0.96	0.92
	1.0	1.03	1.09	1.21	1.32	1.44	1.35	1.25	1.05	0.96	0.92

$(C_N)_{\alpha=60^0}$ as a function of Mach number, aspect ratio & taper ratio

Aspect ratio	Taper ratio	Mach number									
		0	0.6	0.8	1.0	1.2	1.6	2.2	3.0	4.5	≥6.0
≤0.5	0.0	1.10	1.11	1.15	1.26	1.33	1.37	1.31	1.25	1.21	1.18
	0.5	1.26	1.27	1.30	1.40	1.54	1.64	1.54	1.44	1.39	1.36
	1.0	1.26	1.27	1.30	1.40	1.51	1.58	1.54	1.46	1.40	1.36
1.0	0.0	1.44	1.46	1.49	1.53	1.56	1.61	1.50	1.42	1.38	1.36
	0.5	1.40	1.42	1.45	1.53	1.58	1.70	1.64	1.54	1.48	1.45
	1.0	1.33	1.34	1.35	1.44	1.62	1.72	1.67	1.57	1.50	1.46
2.0	0.0	1.26	1.27	1.34	1.48	1.59	1.74	1.68	1.54	1.48	1.45
	0.5	1.30	1.31	1.37	1.48	1.63	1.84	1.80	1.63	1.57	1.54
	1.0	1.30	1.31	1.37	1.48	1.63	1.76	1.73	1.64	1.57	1.54
≥4.0	0.0	1.27	1.28	1.37	1.50	1.64	1.80	1.70	1.56	1.50	1.47
	0.5	1.31	1.32	1.40	1.52	1.70	1.89	1.82	1.66	1.60	1.56
	1.0	1.31	1.32	1.40	1.52	1.70	1.78	1.75	1.66	1.60	1.57

DATA BASE FOR ESTIMATION OF INTERFERENCE FACTOR

TABLE 2(B)

Data for $\left[\Delta K_{f(B)}\right]_{\alpha=0}$ at $\varphi = 0$ deg

Aspect ratio	Taper ratio	Mach number ≤0.1	0.6	0.8	1.2	≥1.5
≤0.25	0, 0.5, 1.0	−0.30	0	0	0	0
0.5	0.5	0.30	0.27	0.23	0.05	0
1.0	0.5	0.54	0.25	0.10	0	0
≥2.0	0.5	0	0.20	0.20	0.10	0
0.5	0	0.30	0.35	0.42	0.18	0
1.0	0	0.54	0.29	0.16	0.06	0
≥2.0	0	0	0.20	0.20	0.10	0
0.5	1.0	0.30	0.27	0.29	0.05	0
1.0	1.0	0.54	0.31	0.19	0.06	0
≥2.0	1.0	0	0.20	0.20	0.10	0

Data for α_C at $\varphi = 0$ deg

Aspect ratio	Taper ratio	Mach number ≤0.1	0.6	0.8	1.2	≥1.5
≤0.25	0, 0.5, 1.0	0	22.0	22.0	0	0
0.5	0.5	30.0	17.3	11.5	10.0	0
1.0	0.5	30.0	15.0	11.0	10.0	0
≥2.0	0.5	10.0	20.0	20.0	15.0	0
0.5	0	30.0	12.0	10.0	10.0	0
1.0	0	30.0	13.0	10.0	10.0	0
≥2.0	0	10.0	20.0	20.0	15.0	0
0.5	1.0	30.0	17.3	15.0	10.0	0
1.0	1.0	30.0	15.0	12.5	10.0	0
≥2.0	1.0	10.0	20.0	20.0	15.0	0

Data for $\left[\Delta K_{f(B)}\right]_{\alpha=\alpha_D}$ at $\varphi = 0$ deg

Aspect ratio	Taper ratio	Mach number ≤0.1	0.6	0.8	1.2	1.5	2.0	2.5	3.0	3.5	4.5	≥5.0
≤0.25	0, 0.5, 1.0	1.0	1.0	1.0	1.0	1.0	1.0	1.0	1.0	1.0	1.0	1.0
0.5	0.5	1.0	1.0	1.0	0.90	0.90	1 0	0.95	1.0	0.97	1.0	1.0
1.0	0.5	1.0	1.0	1.0	0 95	1 0	1 0	1.0	1 0	1 0	1 0	1 0
≥2.0	0.5	1.0	1.0	0.95	0.95	1 0	1.0	1.0	1.0	1.0	1.0	1.0
0.5	0	1.0	1.0	1.0	1.05	0.90	0 90	0.90	0.90	0.90	0 90	1.0
1.0	0	1.0	1.0	1.0	0.95	1 0	1.0	1.0	1 0	1 0	1 0	1.0
≥2.0	0	1.0	1.0	0.95	1.0	1 0	1.0	1.0	1.0	1.0	1.0	1.0
0.5	1.0	1.0	1.0	1.0	1.0	1.0	1.0	1.05	1.15	1.13	1 15	1.0
1.0	1.0	1.0	1.0	1.0	0.95	0.95	0.95	1.0	1.0	1.0	1.0	1.0
≥2.0	1.0	1.0	1.0	1.0	1.0	1.0	1.0	1.0	0.93	0.90	0.95	1.0

Data for α_D at $\varphi = 0$ deg

Aspect ratio	Taper ratio	Mach number									
		≤0.1	0.6	0.8	1.2	1.5	2.0	2.5	3.0	3.5	4.5
≤0.25	0, 0.5, 1.0	44.0	40.0	38.0	35.0	30.0	25.0	16.3	15.1	13.9	13.1
0.5	0.5	50.0	33.0	31.4	27.5	30.0	16.8	17.8	17.0	15.0	15.0
1.0	0.5	50.0	32.5	39.0	22.0	20.0	22.5	17.5	18.0	10.0	17.0
≥2.0	0.5	42.0	35.0	35.0	30.0	25.0	16.5	17.0	16.0	10.0	17.0
0.5	0	50.0	30.0	30.0	21.2	25.0	15.0	14.0	15.0	15.0	12.0
1.0	0	50.0	31.0	39.0	20.0	18.0	21.5	16.0	17.0	11.0	13.0
≥2.0	0	42.0	35.0	35.0	30.0	25.0	20.0	17.7	17.0	12.0	12.6
0.5	1.0	50.0	33.0	34.2	26.0	30.0	14.2	17.0	13.4	11.8	12.2
1.0	1.0	50.0	33.0	40.0	21.0	20.0	22.0	17.0	16 0	9.0	14 0
≥2.0	1.0	42.0	35.0	35.0	30.0	25.0	18.0	15.0	15.5	12.0	12.6

Data for α_M at $\varphi = 0$ deg

Aspect ratio	Taper ratio	Mach number										
		≤0.1	0.6	0.8	1.2	1.5	2.0	2.5	3.0	3.5	4.5	≥5.0
≤0.25	0, 0.5, 1.0	50.0	45.0	45.0	40 0	44.0	38 0	50.0	46.0	50 0	50.0	46.0
0.5	0.5	50.0	33.0	31.4	40.0	50.0	17 0	40 0	17.0	40 0	15.0	14.0
1.0	0 5	50.0	33.0	39.0	45.0	50.0	50.0	50.0	36.0	33 0	17.0	17.0
≥2 0	0.5	50.0	43.0	45.0	30 0	50.0	50.0	50 0	36.0	33 0	17.0	17.0
0.5	0	50.0	30.0	30.0	40.0	50 0	48 0	50 0	50.0	50 0	50.0	50.0
1.0	0	50.0	31.0	40.0	50.0	42.0	50 0	50.0	50.0	44 0	40.0	40.0
≥2.0	0	50.0	43.0	45.0	45.0	50.0	50.0	50.0	50.0	50 0	50.0	35.0
0.5	1.0	50.0	33.0	34.2	50.0	31.0	50 0	50.0	50.0	50 0	50 0	50.0
1.0	1.0	50.0	33.0	40.0	50.0	42.0	50.0	50.0	50.0	44.0	40.0	40.0
≥2.0	1.0	50.0	43.0	45.0	45.0	25.0	18.0	15.0	36.0	33.0	37.0	30.0

Data for $\left[\Delta K_{B(f)}\right]_{\alpha=0}$ at $\varphi = 0$ deg

Aspect ratio	Taper ratio	Mach number										
		≤0.1	0.6	0.8	1.2	1.5	2.0	2.5	3.0	3.5	4.5	≥5.0
≤0.25	0, 0.5, 1.0	0.0	0.0	0.0	0.0	0.0	0.0	0.0	0.0	0.0	0.0	0.0
0.5	0.5	0.0	−0.28	−0.15	0.16	0.10	−0.02	0.0	0.0	0.0	0.0	0.0
1.0	0.5	0.0	−0.20	−0.20	0.15	0 20	0.05	0.0	0.0	0.0	0.0	0.0
≥2.0	0.5	0.0	−0.20	−0 07	0.17	0.18	0.10	0 0	0.0	0.0	0.0	0.0
0.5	0	0.0	−0.33	−0.30	0.28	0.20	0.10	0.08	0.0	0.0	0.0	0.0
1.0	0	0.0	−0.24	−0.25	0.13	0.28	0 05	0 0	0 0	0 0	0.0	0.0
≥2.0	0	0.0	−0 20	−0.07	0.17	0 0	0.05	0.0	0 0	0.0	0.0	0.0
0.5	1.0	0.0	−0.28	−0.15	0.25	0.0	0.10	0 0	0.0	0.0	0 0	0.0
1.0	1.0	0.0	−0.20	−0.20	0.22	0 10	0.05	0 0	0.0	0.0	0.0	0.0
≥2.0	1.0	0.0	−0.20	−0.07	0.17	0.20	0.10	0.15	0.0	0.0	0.0	0.0

Data for $\frac{dK_{f(B)}}{d\alpha}$ at $\varphi = 0$ deg

Aspect ratio	Taper ratio	Mach number									
		≤ 0.1	0 6	0.8	1.2	1.5	2 0	2.5	.30	3.5	4.5	≥ 5.0
≤ 0.25	0, 0.5, 1.0	0.0	0.0	0.0	0.0	0 0	0 0	−0.007	−0.014	−0.015	−0.02	−0.024
0.5	0.5	0.006	0 023	0.023	−0 009	−0 012	−0 010	−0 015	−0 014	−0.015	−0 016	−0.020
1 0	0 5	0 006	0 012	0 011	−0 003	−0 003	−0 005	−0 006	−0.008	−0.010	−0 012	−0.015
≥ 2 0	0.5	0.0	0.012	0.011	0 0	0.0	−0 001	−0 012	−0.014	−0.015	−0.016	−0.020
0.5	0	0.006	0.043	0.058	0.0	0.0	0 0	−0 004	−0 014	−0.015	−0.016	−0.020
1.0	0	0.006	0.020	0 0225	−0.003	−0.003	−0.005	−0 006	−0 008	−0.010	−0.012	−0.015
≥ 2.0	0	0 0	0 012	0 011	0 0	0 0	−0 002	−0 012	−0 014	−0.015	−0 016	−0.020
0 5	1.0	0 006	0 038	0 033	−0 013	−0 012	−0 010	−0 015	−0.014	−0.015	−0.016	−0.020
1 0	1.0	0 006	0 007	0.005	−0.003	−0.010	−0.010	−0 015	−0.016	−0.016	−0.016	−0.018
≥ 2 0	1.0	0.0	0.012	0.011	0 0	−0.002	−0 007	−0 012	−0.014	−0.015	−0.016	−0.020

Data for α_1 at $\varphi = 0$ deg

Aspect ratio	Taper ratio	Mach number										
		≤0 1	0.6	0 8	1.2	1.5	2.0	2.5	3.0	3 5	4.5	≥5 0
≤0.25	0, 0.5, 1 0	30.0	21.1	16.5	45.0	37.0	33.3	23.3	20.5	18.0	15.0	14.0
0.5	0.5	30 0	22.2	16 7	62 0	43.0	40 0	25 0	25 0	25.0	20 0	20.0
1.0	0.5	30 0	25.0	20 0	70.0	30.0	25.0	28.6	23 0	20.4	26 0	26 0
≥2 0	0.5	30 0	25 0	20 0	40 0	66.0	58.0	30 0	24.0	20 4	26 0	26.0
0.5	0	30 0	24.2	17 2	25.0	25.0	20.0	20.0	10.0	27.0	20.0	20.0
1.0	0	30 0	25.0	20 0	70.0	61.0	18 0	27.0	18 0	24 0	24.0	24.0
≥2 0	0	30 0	25.0	20.0	40.0	48.5	49 0	30 0	32 0	30.0	26 0	26.0
0 5	1.0	30.0	17.0	15.5	48 5	43 0	40.0	25.0	26.5	21.6	20.0	20.0
1 0	1 0	30.0	25 0	20 0	70 0	54.0	22.0	29.5	23.5	18.0	22.0	22.0
≥2.0	1.0	30.0	25.0	20.0	40.0	48 0	47.0	32.0	26 0	20 0	26.0	26.0

Data for α_2 at $\varphi = 0$ deg

Aspect ratio	Taper ratio	Mach number										
		≤0.1	0.6	0.8	1.2	1.5	2.0	2.5	3.0	3.5	4.5	≥5.0
≤0.25	0, 0.5 1.0	90 0	80.0	65.0	63.4	45.0	43.3	42.5	31.5	37.3	40.0	40.0
0.5	0.5	90 0	80.0	65 0	62.0	43.0	41 0	42.5	25.0	42.0	40.0	40.0
1.0	0.5	90 0	80.0	80.0	80.0	65 0	46.0	40.0	36 0	40 0	40 0	40.0
≥2.0	0.5	90.0	80.0	80.0	80.0	90.0	90.0	42.0	40.0	40.0	40.0	40.0
0.5	0	90.0	80.0	80.0	80.0	49 0	47.8	42.5	43 0	26.5	40.0	40.0
1.0	0	90.0	80.0	80.0	80.0	59.0	46.0	40.0	40.0	34.0	40.0	40.0
≥2.0	0	90.0	80 0	80.0	80.0	90.0	90.0	41.0	35.0	40.0	43.0	43.0
0.5	1.0	90.0	80.0	53.2	48.7	43.0	41.0	42.5	26.5	43.5	40.0	40.0
1.0	1.0	90.0	80.0	74.0	72.0	55.0	46.0	40 0	32.0	40.0	40.0	40.0
≥2.0	1.0	90.0	80.0	80.0	80.0	90.0	90.0	45.0	30.0	40.0	43.0	43.0

APPENDIX 'B'

PROCESSING OF WIND TUNNEL DATA

Two sets of test were undertaken

1.Dry run

2.Wind run.

Both these sets were carried out for three configurations:

1.Body alone

2.Body + fin for delta=0

3.Body + fin for delta=-40,-35,-30,-25,-20,-10,+10.

The dry run for all the above three configurations are considered offsets and are subtracted from each of the values of wind run.

Thus a new set of corrected values of $c1, c2, c3, c4, c5, c6$ in voltage form is obtained which is processed to obtain forces and moments and their respective coefficients. A detailed procedure is described below.

The wind tunnel data was obtained at the balance center in the form of $c1, c2, c3, c4, c5, c6$ in voltage form. Also the slope was obtained.

If

y=output from wind tunnel in voltage form.

m=slope(given)

x=force (kgf) or moment (kgf-m)

Thus the values of forces and moments $axf, n1, n2, s1, s2, rm$ in kgf and kgf-m respectively were obtained by solving the equation :

y=mx

Thus following data was obtained w.r.t the balance center.

Sign Convention(For tunnel axes)

1) positive x is towards tail .
2) Positive y is rightward as viewed from rear.
3) Positive z is upward.

Sign Convention(For Trajectory axes)

1)Positive x is towards Nose.

2)Positive y is rightward as viewed from rear.

3)Positive z is Downward.

Also it should be noted:

$$F_N = -F_Z$$
$$F_X = -F_A$$

Step 1.

Force (balance center)

$$(F_x)_{balance} = -axf$$
$$(F_N)_{balance} = -(n1+n2)$$
$$(F_Y)_{balance} = s1+s2$$

Moment (balance center)

$$(Pm)_{balance} = -(n1-n2)\times 0.065$$
$$(Ym)_{balance} = (s1-s2)\times 0.065$$
$$(Rm)_{balance} = rm$$

Step 2.

It should be noted that the above values are w.r.t the balance center. These needed to be transformed to the model center of gravity.

The distance between the balance center and the model cg was calculated and thus if xd is the distance of balance center and model cg then the following equations are used to transform the force and moments from balance center to model c.g

Force Transformation from balance center to model center of gravity

$$(F_x)_{cg} = (F_x)_{balance}$$

$$(F_N)_{cg} = (F_N)_{balance}$$

$$(F_Y)_{cg} = (F_Y)_{balance}$$

Moment Transformation from balance center to model center of gravity

$$(Pm)_{cg} = (Pm)_{balance} - (F_N)_{balance}.xd$$

$$(Ym)_{cg} = (Ym)_{balance} - (F_Y)_{balance}.xd$$

$$(Rm)_{cg} = (Rm)_{balance}$$

Step 3.

The next step was to evaluate the forces and moment coefficients.

$$C_X = \frac{(F_x)_{cg}.9.81}{0.5\rho V^2 S_{ref}}$$

$$C_Y = \frac{(F_Y)_{cg}.9.81}{0.5\rho V^2 S_{ref}}$$

$$C_N = \frac{(F_N)_{cg}.9.81}{0.5\rho V^2 S_{ref}}$$

$$C_m = \frac{(Pm)_{cg}.9.81}{0.5\rho V^2 S_{ref}.d}$$

$$C_n = \frac{(Ym)_{cg}.9.81}{0.5\rho V^2 S_{ref}.d}$$

$$C_l = \frac{(Rm)_{cg}.9.81}{0.5\rho V^2 S_{ref}.d}$$

Step 4

The next step is to transform the body axes coefficients to wind axes .

Force Transformation from Body to Wind Axes

$$D = (F_X)_{cg}\cos\alpha\cos\psi + (F_N)_{cg}\sin\alpha\cos\psi + (F_Y)_{cg}\sin\psi$$

$$L = (F_N)_{cg}\cos\alpha\cos\phi - (F_X)_{cg}\sin\alpha\cos\phi - (F_Y)_{cg}\cos\psi\sin\phi + (F_X)_{cg}\sin\psi\sin\phi$$

$$Y = (F_Y)_{cg}\cos\psi\cos\phi - (F_X)_{cg}\sin\psi\cos\phi - (F_N)_{cg}\cos\alpha\sin\phi - (F_X)_{cg}\sin\alpha\sin\phi$$

Moment Transformation from Body to Wind Axes

$$Pm = (Pm)_{cg}\cos\psi\cos\phi + (Rm)_{cg}\sin\psi\cos\alpha\cos\phi + (Ym)_{cg}\sin\alpha\sin\psi\cos\phi$$
$$-(Ym)_{cg}\cos\alpha\sin\phi + (Rm)_{cg}\sin\alpha\sin\phi$$

$$Ym = (Ym)_{cg}\cos\alpha\cos\phi - (Rm)_{cg}\sin\alpha\cos\psi + (Pm)_{cg}\cos\psi\sin\phi$$
$$+(Rm)_{cg}\cos\alpha\sin\phi\sin\psi + (Ym)_{cg}\sin\alpha\sin\psi\sin\phi$$

$$Rm = (Rm)_{cg}\cos\alpha\cos\psi + (Ym)_{cg}\sin\alpha\cos\psi - (Pm)_{cg}\sin\psi$$

Step 5

Conversion of Wind Axes Forces and Moments to Coefficient Form:

Force Coefficient

$$C_L = \frac{L\times 9.81}{0.5\rho V^2 S_{ref}}$$

$$C_D = \frac{D \times 9.81}{0.5\rho V^2 S_{ref}}$$

$$C_Y = \frac{Y \times 9.81}{0.5\rho V^2 S_{ref}}$$

Moment Coefficient

$$C_m = \frac{Pm \times 9.81}{0.5\rho V^2 S_{ref} .d}$$

$$C_n = \frac{Ym \times 9.81}{0.5\rho V^2 S_{ref} .d}$$

$$C_l = \frac{Rm \times 9.81}{0.5\rho V^2 S_{ref} .d}$$

Thus body axes coefficients $C_X, C_Y, C_N, C_m, C_n, C_l$ and wind axes coefficients $C_D, C_Y, C_L, C_m, C_n, C_l$ are obtained for each of the configurations discussed previously as a function of angle of attack.

Let us now denote the body axes coefficients obtained after processing the raw wind tunnel data for three configurations namely:

1. *body alone*

$$(C_N)_{body} = C_N$$
$$(C_X)_{body} = C_X$$
$$(C_Y)_{body} = C_Y$$
$$(C_m)_{body} = C_m$$
$$(C_n)_{body} = C_n$$
$$(C_l)_{body} = C_l$$

2. $(body + fin)_{\delta=0}$

$$(C_N)_{(body+fin)_{\delta=0}} = C_N$$

$(C_X)_{(body+fin)_{\delta=0}} = C_X$

$(C_Y)_{(body+fin)_{\delta=0}} = C_Y$

$(C_m)_{(body+fin)_{\delta=0}} = C_m$

$(C_n)_{(body+fin)_{\delta=0}} = C_n$

$(C_l)_{(body+fin)_{\delta=0}} = C_l$

3. $(body + fin)_{\delta=\delta 1}$

$(C_N)_{(body+fin)_{\delta=\delta 1}} = C_N$

$(C_X)_{(body+fin)_{\delta=\delta 1}} = C_X$

$(C_Y)_{(body+fin)_{\delta=\delta 1}} = C_Y$

$(C_m)_{(body+fin)_{\delta=\delta 1}} = C_m$

$(C_n)_{(body+fin)_{\delta=\delta 1}} = C_n$

$(C_l)_{(body+fin)_{\delta=\delta 1}} = C_l$

The next step was to develop a mathematical model, which can evaluate the stability derivatives

Longitudinal derivatives: $C_{N\alpha}, C_{N\delta}, C_{Nq}, C_{m\alpha}, C_{mq}, C_{m\delta}$

Lateral Derivatives: $C_{y\beta}, C_{y\delta r}, C_{yp}, C_{yr}, C_{n\beta}, C_{nr}, C_{np}, C_{n\delta r}$
$C_{l\beta}, C_{l\delta a}, C_{lp}, C_{lr}$

Since the test was carried out for

1.Body alone

2.Body + fin for delta=0

3.Body + fin for delta=-40,-35,-30,-25,-20,-10,+10.

Thus we have assumed that all the stability derivatives are composed of the contribution from:

i) *body alone*

ii) $(body + fin)_{\delta=0}$

iii) $(body + fin)_{\delta=\delta 1}$

Thus

$$C_N = (C_N)_{body} + (C_N)_{(fin)_{\delta=0}} + (C_N)_{(fin)_{\delta=\delta 1}}$$
$$C_X = (C_X)_{body} + (C_X)_{(fin)_{\delta=0}} + (C_X)_{(fin)_{\delta=\delta 1}}$$
$$C_Y = (C_Y)_{body} + (C_Y)_{(fin)_{\delta=0}} + (C_Y)_{(fin)_{\delta=\delta 1}}$$
$$C_m = (C_m)_{body} + (C_m)_{(fin)_{\delta=0}} + (C_m)_{(fin)_{\delta=\delta 1}}$$
$$C_l = (C_l)_{body} + (C_l)_{(fin)_{\delta=0}} + (C_l)_{(fin)_{\delta=\delta 1}}$$
$$C_n = (C_n)_{body} + (C_n)_{(fin)_{\delta=0}} + (C_n)_{(fin)_{\delta=\delta 1}}$$

Stability Derivatives From Body Alone

In order to evaluate $(C_{N\alpha})_{body}, (C_{Y\beta})_{body}, (C_{m\alpha})_{body}, (C_{l\beta})_{body}, (C_{n\alpha})_{body}$ the data from the wind tunnel in coefficient form was further resolved into individual components.

$$(C_N)_{body} = (C_{N\alpha})_{body}.\alpha$$

Since we have the body axes force coefficients and moment coefficients $C_X, C_Y, C_N, C_m, C_n, C_l$ from the wind tunnel.

$$(C_{N\alpha})_{body} = \frac{(C_N)_{body}}{\alpha}$$
$$(C_{m\alpha})_{body} = \frac{(C_m)_{body}}{\alpha}$$
$$(C_{N\beta})_{body} = -(C_{N\alpha})_{body}$$
$$(C_{Nq})_{body} = -2.(C_{N\alpha})_{body}.\frac{(xcg - xcp_{body})}{d}$$

Stability derivatives from Body + fin at $\delta = 0$

$$(C_N)_{(fin)_{\delta=0}} = (C_N)_{(body+fin)_{\delta=0}} - (C_N)_{body}$$
$$(C_m)_{(fin)_{\delta=0}} = (C_m)_{(body+fin)_{\delta=0}} - (C_m)_{body}$$

Let $(C_N)_{(fin)_{\delta=0}} = (C_N)_{fin}$

$$(C_{N\alpha})_{fin} = \frac{(C_N)_{fin}}{\alpha}$$

$$(C_{m\alpha})_{fin} = \frac{(C_m)_{fin}}{\alpha}$$

$$(C_{Nq})_{fin} = -2.(C_{N\alpha})_{fin}.\frac{(xcg - xcp_{fin})}{d}$$

$$(C_{mq})_{fin} = -2.(C_{m\alpha})_{fin}.\left(\frac{xcg - xcp_{fin}}{d}\right)^2$$

$$(C_{n\beta})_{fin} = -(C_{m\alpha})_{fin}$$

$$(C_{y\beta})_{fin} = -(C_{N\alpha})_{fin}$$

$$(C_{yr})_{fin} = -2.(C_{n\beta})_{fin}.\frac{(xcg - xcp_{fin})}{d}$$

$$(C_{yp})_{fin} = -2.(C_{n\beta})_{fin}.\frac{\overline{R}}{d}$$

$$C_{np} = -2.15.(C_{N\alpha})_{fin}.\left(\frac{\overline{R}}{d}\right)^2.2$$

Stability Derivatives From Body + Fin at $\delta = \delta 1$ (-40, -35, -30, -25, -20, -10, +10)

$$(C_N)_{(fin)_{\delta=\delta 1}} = (C_N)_{(body+fin)_{\delta=\delta 1}} - (C_N)_{(fin)_{\delta=0}} - (C_N)_{body}$$

$$(C_m)_{(fin)_{\delta=\delta 1}} = (C_m)_{(body+fin)_{\delta=\delta 1}} - (C_m)_{(fin)_{\delta=0}} - (C_m)_{body}$$

Let

$\delta 1 = \delta$

$$(C_N)_{(fin)_{\delta=\delta 1}} = (C_N)_{\delta}$$

$$(C_m)_{(fin)_{\delta=\delta 1}} = (C_m)_{\delta}$$

$$C_{N\delta} = \frac{(C_N)_{\delta}}{\delta 1}$$

$$C_{m\delta} = \frac{(C_m)_{\delta}}{\delta}$$

$$C_{y\delta r} = -C_{N\delta}$$

$$C_{n\delta r} = -C_{m\delta}$$

$$C_{n\delta r} = C_{m\delta}$$

In sum the total derivatives discussed can be written in summation form as

$$C_{N\alpha} = (C_{N\alpha})_{body} + (C_{N\alpha})_{fin}$$
$$C_{m\alpha} = (C_{m\alpha})_{body} + (C_{m\alpha})_{fin}$$
$$C_{mq} = (C_{mq})_{body} + (C_{mq})_{fin}$$
$$C_{Nq} = (C_{Nq})_{body} + (C_{Nq})_{fin}$$
$$C_{y\beta} = (C_{y\beta})_{body} + (C_{y\beta})_{fin}$$
$$C_{yr} = (C_{yr})_{body} + (C_{yr})_{fin}$$
$$C_{yp} = (C_{yp})_{body} + (C_{yp})_{fin}$$
$$C_{n\beta} = (C_{n\beta})_{body} + (C_{n\beta})_{fin}$$

Futher

$$C_{mi} = C_{mq}$$

$$C_{lr} = 2.C_{y\beta}.\left(\frac{xcg - xcp_{fin}}{d}\right)^2$$

$$C_{l\delta r} = (C_{N\alpha})_{fin}.\left(\frac{\bar{R}}{d}\right)^2$$

$$C_{l\delta\alpha} = (C_{N\alpha})_{fin}.\frac{\bar{R}}{d}$$

Thus the final model used in the trajectory modeling including the damping derivatives

$$C_N = C_{N\alpha}.\alpha + C_{N\delta}.\delta + C_{Nq}.\frac{qd}{2v}$$

$$C_A = C_{A\alpha}.\alpha + C_{A\delta}.\delta + C_{Aq}.\frac{qd}{2v}$$

$$C_m = C_{m\alpha}.\alpha + C_{m\delta}.\delta + C_{mq}.\frac{qd}{2v}$$

$$C_Y = C_{y\beta}.\beta + C_{y\delta}.\delta + C_{yp}.\frac{pd}{2v} + C_{yr}.\frac{rd}{2v} + C_{\delta r}.\frac{rd}{2v}$$

$$C_l = C_{l\beta}.\beta + C_{l\delta a}.\delta a + C_{lp}.\frac{pd}{2v} + C_{lr}.\frac{rd}{2v} + C_{\delta r}.\delta r$$

$$C_n = C_{n\beta}.\beta + C_{nr}.\frac{rd}{2v} + C_{n\delta}.\delta + C_{np}.\frac{pd}{2v} + C_{n\delta r}.\frac{rd}{2v}$$

These derivatives can be used in the trajectory modeling. The derivatives are obtained as a function of angle of attack.